ABSTRACT

MODELING, SIMULATION AND HEMODYNAMIC RESPONSE ANALYSIS OF ARTERIOVENOUS MALFORMATION OCCLUSION

by
Huijuan Mao

The cerebral Arteriovenous Malformation system(AVM) or
fistula, is a network with large caliber vessels that yields
an alternate pathway for blood flow between arteries and
veins. Neurosurgical and interventional radiological
techniques are the common way to treat AVM patients so that
the normal capillary blood flow would be restored. Several
patients who underwent this procedure had different degrees
of brain swelling and subsequent hemorrhage. To understand
this, Blesser et al. developed a simplified model to
simulate the effect of AVM occlusion on cerebrovascular
pressure and flow. Their model does not include the
cerebrovascular regulatory mechanism which is an important
part in cerebral pressure and flow regulation. Three
different factors that may affect the hemodynamic response
after AVM occlusion were investigated in this work. They
are: autoregulation mechanism failure, sympathetic nervous
system dysfunction and increased intracranial pressure. The
revised model predicted the relationship between each of
these three factors and the severity of the hemorrhage. The
simulation results predicted that autoregulation mechanism

dysfunction is the most important factor of all three factors, whereas increased intracranial pressure is the least important factor. Possible future study would include developing a model where autoregulation failure and sympathetic system dysfunction are considered simultaneously and the addition of other possible pathologies such as the failure of chemical regulation mechanisms, and to investigate the relationship between these factors and the potential for hemorrhage.

MODELING, SIMULATION AND HEMODYNAMIC RESPONSE ANALYSIS OF
ARTERIOVENOUS MALFORMATION OCCLUSION

by
Huijuan Mao

A Thesis
Submitted to the Faculty of
New Jersey Institute of Technology
in Partial Fulfillment of the Requirement for the Degree of
Master of Science in Biomedical Engineering

Biomedical Engineering Committee

May 1994

Blank Page

APPROVAL PAGE

MODELING, SIMULATION AND HEMODYNAMIC RESPONSE ANALYSIS OF
ARTERIOVENOUS MALFORMATION OCCLUSION

Huijuan Mao

Dr. Stanley Reisman, Thesis Advisor   Date
Professor of Electrical and
Computer Engineering, NJIT

Dr. David Kristol, Committee Member   Date
Professor of Chemistry, Director and Graduate
Advisor of Biomedical Engineering, NJIT

Dr. Peter Engler, Committee Member   Date
Associate Professor of Electrical and
Computer Engineering, NJIT

BIOGRAPHICAL SKETCH

Author: Huijuan Mao

Degree: Master of Science in Biomedical Engineering

Date: May 1994

Undergraduate and Graduate Education

- Master of Science in Biomedical Engineering,
  New Jersey Institute of Technology,
  Newark, New Jersey, 1994

- Bachelor of Engineering in Biomedical Engineering,
  Shanghai Medical University,
  Shanghai, P.R.China,1984

Major: Biomedical Engineering

Presentation and Publications:

Mao H.J. and Reisman S., "Modeling and Computer Simulation of the Effect of Degree of Autoregulation on Arteriovenous Malformation Occlusion." Proceedings of the 20th IEEE Northeast Bioengineering Conference, 1994, pp.46-47.

ACKNOWLEDGMENT

This thesis is dedicated to
my dear parents and my family.

TABLE OF CONTENTS

LIST OF FIGURES

LIST OF TABLES

CHAPTER 1

INTRODUCTION

1.1 Basic Concept of AVM

The cerebral arteriovenous malformation (AVM) system or fistula, in its general form, is a network with large caliber vessels that yields an alternate pathway for blood flow between arteries and veins. It consists of a feeding artery, AVM core, draining vein and capillary bed which is juxtaposed in parallel with the AVM as shown in figure.1.1, [1] [7]
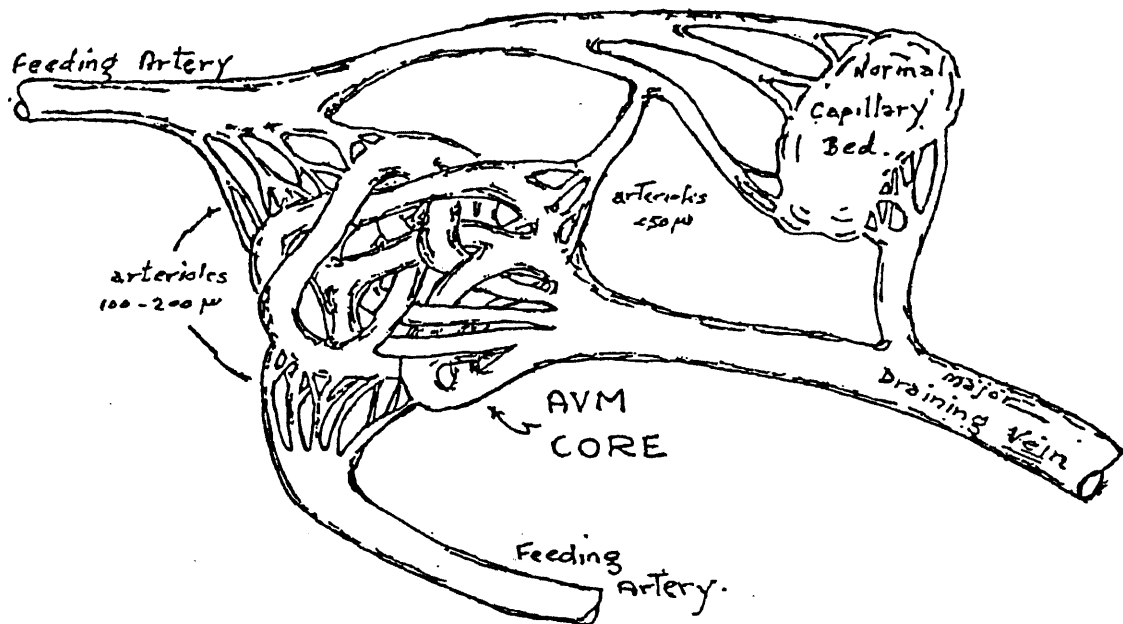
Figure.1.1 Physiologic Representation of AVM System

where the feeding artery supplies blood to both capillary bed and AVM core, and then converges into a draining vein. We know that normal blood circulation begins at the feeding artery, through the capillary bed, to the draining vein, whereas in AVM patients, there are some additional vessels existing between the feeding artery and the draining vein. Also, because of their large caliber compared to the capillary bed, AVMs usually have a lower intravascular resistance. This produces high-flow and low-pressure characteristics, and shunts most of the flow from the physiological capillary beds. Thus this nonnutritional pathway actually "steals" the blood away from capillary beds and reduces the blood supply to normal brain tissue adjacent to the AVM core. As a result, varying degrees of cerebral ischemia and central nervous system dysfunction occur. To treat these cases, neurosurgical and interventional radiological techniques are used to surgically resect and gradually embolize the AVM core so that the normal capillary blood flow would be restored. Unfortunately, several patients who underwent this procedure suffered from variable degrees of brain swelling and hemorrhage after AVM occlusion[2] [3]. The precise mechanisms for this swelling are still poorly understood, though a variety of research is currently underway. One hypothesis[3] suggests that decreased perfusion in the surrounding normal brain sharing the same circulation leads to a state of vasomotor paresis, that is , autoregulation mechanism failure, and that , after

AVM resection, blood from the AVM vascular bed is routed into previously underperfused vasculature which is unable to autoregulate effectively. This causes the capillary bed to be acutely overloaded and may lead to edema or hemorrhage.

1.2 AVM Modeling Consideration

In order to better understand this abnormal result, Blesser et al developed a simplified computer model to simulate the hemodynamic response of the cerebral circulation to AVM embolization[1]. Their model has been used to qualitatively simulate some of the observed alterations in pressure and flow resulting from AVM occlusion. In a recent study, it was found that the hemodynamic response of AVM occlusion varies in individuals[1][2] and may be affected by many factors[8] such as cerebral autoregulation function and sympathetic nervous system function. Thus, a hemodynamic response analysis incorporating these different factors following AVM occlusion will be helpful to discover the reasons behind the aforementioned problems. In this paper we investigate three possible factors which are (1) different degrees of autoregulation mechanism .failure (2) sympathetic nervous system dysfunction and (3) patients having increased intracranial pressure.

CHAPTER 2

MODELING BACKGROUND

2.1 Original Model Construction

It was found in a recent study that about 18% of AVM patients will develop hyperemia and subsequent hemorrhage which is the major cause of postoperative morbidity and mortality[1][2], The precise mechanisms are poorly understood, although a shunting of blood through a nonnutritional pathway with associated hypoperfusion of adjacent tissue is likely. In general, AVMs have an intravascular resistance to flow lower than that of the surrounding brain vasculature[1][2], resulting in a high flow/low resistance system. This may lead to decreased perfusion to the surrounding normal brain tissue sharing the same circulation. The high nonnutritive flows into the AVM are thought to create a "steal" phenomenon. Several lines of evidence have implicated the significant preoperative steal as an important pathophysiological event[6]. With removal of the AVM, this "steal" is reversed, and marginally perfused tissue receives a proportionally greater flow. If the adjacent areas have been chronically ischemic, they may have lost the ability to autoregulate[1][2]. If this is the case, removal of the AVM will result in high flows into these areas of brain with diminished or absent autoregulation and subsequent hyperperfusion injury, i.e.,

4

cerebral swelling or intracerebral hemorrhage. In order to better understand the effect of progressive AVM occlusion on cerebrovascular pressure and flow, Blesser et al have developed a simplified model of the AVM configuration which was simulated on a 486-based personal computer using the VisSim (Visual solutions Inc.,Westford, MA) graphical modeling program[Appendix]. To simplify the simulation procedure in their model, the AVM system (figure 1.1) was simplified and rearranged as shown in figure 2.1, where two feeding arteries are considered as one and some very small shunts from the capillary bed to the AVM core are neglected.
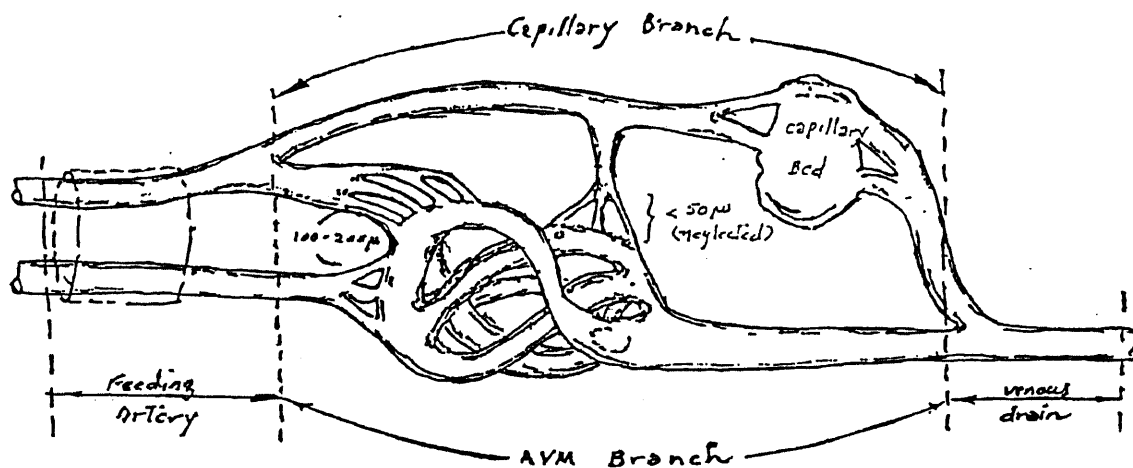
Figure 2.1 Rearranged Representation of AVM System

Based on this simplified diagram, a mechanical equivalent circuit is derived as shown in figure 2.2, where each branch can be modeled with a 'tube' and an elastic 'ball' representing the compliance of the vessel. The feeding artery supplies the blood to both capillary bed and fistula-

like AVM branch and both empty into a draining vein. Electrically, each branch can be represented by two separate lumped proximal and distal resistors and a capacitor representing the compliance of the vessel. The electrical analog circuit of the total system can be
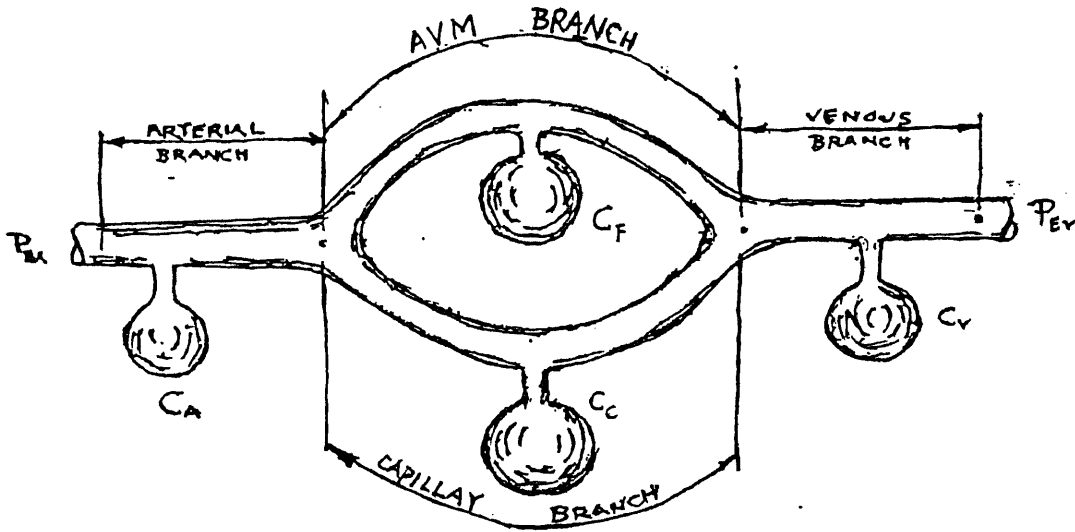
Figure 2.2 The Mechanical Equivalent of AVM System
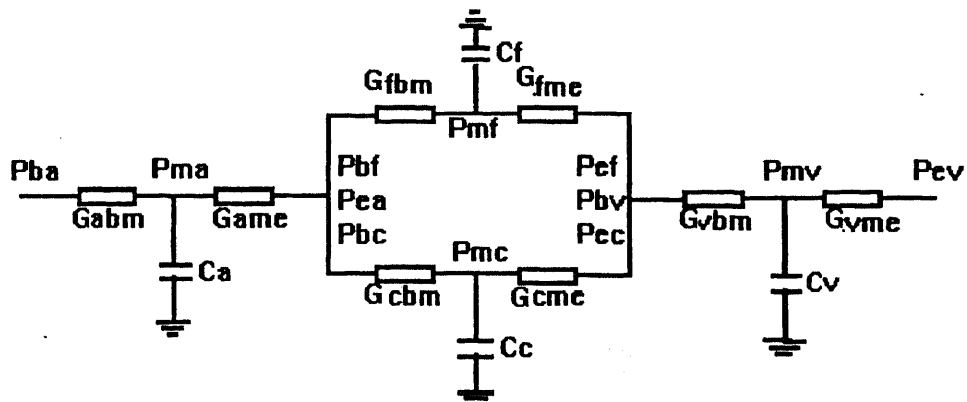
Figure 2.3 Electrical Equivalent of AVM System

represented by figure 2.3. Subscripts in the figures denote the following: a = feeding artery, f = fistula, c = capillary bed, v = draining vein, b, m, e = the beginning, middle and end of the aforementioned vessel segment respectively. All resistors are considered to be nonlinear and pressure dependent, satisfying the Hagen-Poiseulle's equation, where blood flow(Q) is directly related to the pressure difference(ΔP) and the fourth power of radius(r), and is inversely related to the length of vessel(L) and viscosity(η). The equation is expressed as

$$Q = \frac{\Delta P \pi r^4}{8 \eta L}$$ (2.1)

Note that the resistance of the vessel $R = \frac{\Delta P}{Q} = \frac{8 \eta L}{\pi r^4}$ is a function of the vessel radius which is assumed pressure dependent. A set of equations can be derived from the electric circuit (figure 2.3). We can begin from a typical branch which is represented by figure 2.4.
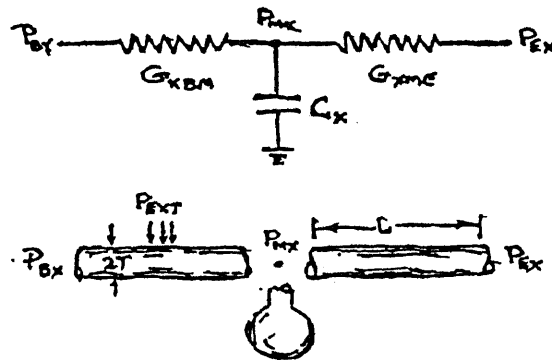
Figure 2.4   Electrical and Mechanical
Representation of a Typical Branch

Kirchoff's Current Law at the central node produces:

$$(P_{BX} - p_{MX})G_{XBM} = C_X P_{MX} + (P_{MX} - P_{EX})G_{XME} \qquad (2.2)$$

or $\quad P_{BX}G_{XBM} + P_{EX}G_{XME} = C_X P_{MX} + P_{MX}(G_{XME} + G_{XBM}) \qquad (2.3)$

where a general conductance

$$Gxyz = \frac{\pi r^4}{8L\eta} \qquad (2.4)$$

and r = tube radius, L = tube length, η = blood viscosity. Therefore, the conductance Gxyz is a function of the tube radius (r) which is further a function of the transmural pressure Ptrx, which is defined as the pressure difference between vessel internal and external pressure, and is expressed mathematically as,

$$G = K (r) = K [f(Ptrx)] \qquad (2.5)$$

From the mechanical representation shown in figure 2.4

$$Ptrx = (\frac{Pbx + Pmx}{2} - P_{external}) \qquad (2.6)$$

If the ambient pressure(approximated as Pext) is neglected, then the transmural pressure would only be a function of the average internal pressure Pav,

that is $\qquad Ptrx = \frac{Pbx + Pmx}{2} = Pav \qquad (2.7)$

The simulation block diagram for the typical branch can be developed from equations(2.3)to(2.7)and is shown in figure

2.5. In the figure, P_{BX} is the known input source, and the left side from A to B represents equation(2.3), where G_{SUM} is the sum of G_{XBM} and G_{XME}. The right side represents the derivation of the nonlinearity of the vessel conductance G_{XBM} and G_{XME} which are represented by equation(2.7),(2.5),(2.4). In order to combine the four branches together, the other three branch equations can be derived in a similar way. We therefore obtain for the four branches:

$$\textit{Artery:} \quad P_{ba}G_{abm} + P_{ea}G_{ame} = C_a\dot{P}_{ma} + P_{ma}(G_{ame} + G_{abm}) \qquad (2.8)$$

$$\textit{Capillary:} \quad P_{bc}G_{cbm} + P_{ec}G_{cbm} = C_c\dot{P}_{mc} + P_{mc}(G_{cme} + G_{cbm}) \qquad (2.9)$$

$$\textit{Fistula} \quad P_{bf}G_{fbm} + P_{ef}G_{fme} = C_f\dot{P}_{mf} + P_{mf}(G_{fme} + G_{fbm}) \qquad (2.10)$$

$$\textit{Vein:} \quad P_{bv}G_{vbm} + P_{ev}G_{vme} = C_v\dot{P}_{mv} + P_{mv}(G_{vme} + G_{vbm}) \qquad (2.11)$$

$$\textit{Note that} \qquad P_{ea} = P_{bc} = P_{bf}$$

$$\textit{and} \qquad P_{bv} = P_{ec} = P_{ef}$$
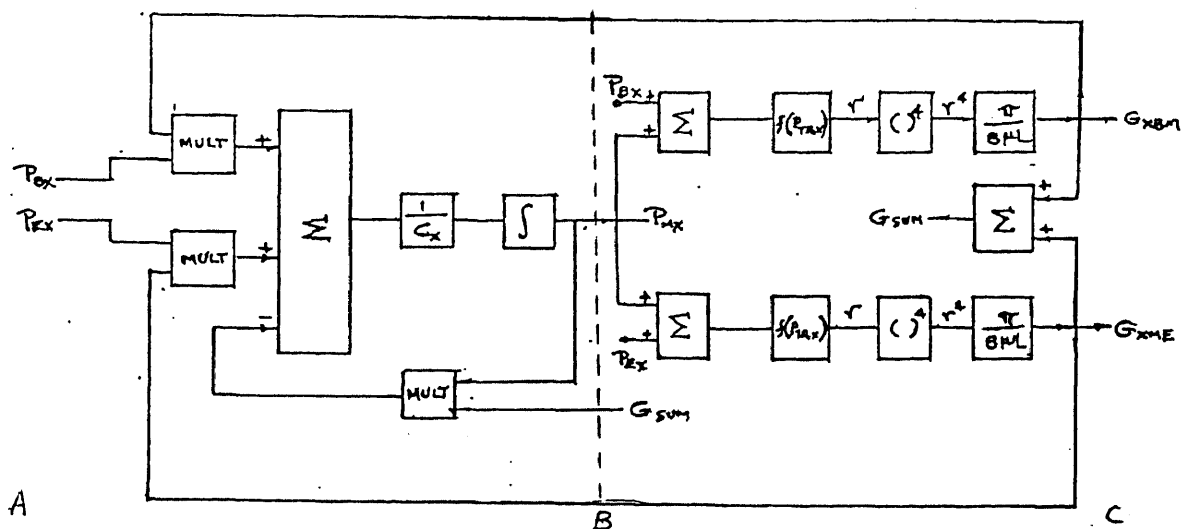
Figure 2.5 Block Diagram for a Typical Branch

Four equations are not enough to solve for the six unknowns Pma, Pea, Pmc, Pmf, Pbv and Pmv, so another two equations are needed. These are written at the branch confluent and effluent points:

$$P_{ea} = \frac{P_{ma}G_{ame} + P_{mc}G_{abm} + P_{mf}G_{fbm}}{G_{ame} + G_{fbm} + G_{fme}} \qquad (2.12)$$

$$P_{bv} = \frac{P_{mf}G_{fme} + P_{mc}G_{cme} + P_{mv}G_{vbm}}{G_{vbm} + G_{cme} + G_{fme}} \qquad (2.13)$$

The six equations are enough to solve for the six unknowns. The total system block diagram is shown in figure 2.6, where the four branches, artery, capillary, fistula and

2.6, where the four branches, artery, capillary, fistula and vein are treated as four compound blocks[Appendix] which are similar to the typical branch shown in figure 2.5. The source in figure 2.6 is a simulated feeding artery pressure wave that varies from 35 to 50 mmHg, and the sink pressure is assumed to be 5 mmHg. In order to include these diagram into VisSim, Dr. W.Blesser estimated the various system parameters through many experiments so that the simulation of the model will produce physiologically meaningful results.

2.2 Parameter Estimation

(1). Estimation of the conductance constants

It is assumed, in Blesser's model, that the branch resistive effects are nonlinear and that they are a function of changes in diameter due to the transmural pressures. From the Poiseuille's equation, $Q = \dfrac{\Delta P \pi r^4}{8 \eta L}$, the branch conductance can be expressed by:

$$G = \frac{\pi r^4}{8L\eta} = Kr^4 \qquad \text{or} \qquad K = \frac{G}{r^4} \qquad (2.14)$$

The proportionality constant, K, can be determined if some estimation for the branch resistance or conductance (G) and the radius (r) are assumed. The branch resistance can be approximated from the expected pressure drops across them.

For example Blesser assumed the blood flow (Q) in the feeding artery is 50 ml/min./100g, and expected pressure drops from Pba to Pma at quiescence (ΔP) can be calculated as follows:

Assume   Pma = 32mmHg [7]

We know   Pba = 1/2(35+50)=42.5 mmHg

Thus ΔP = 42.5-32 = 10.5 mmHg
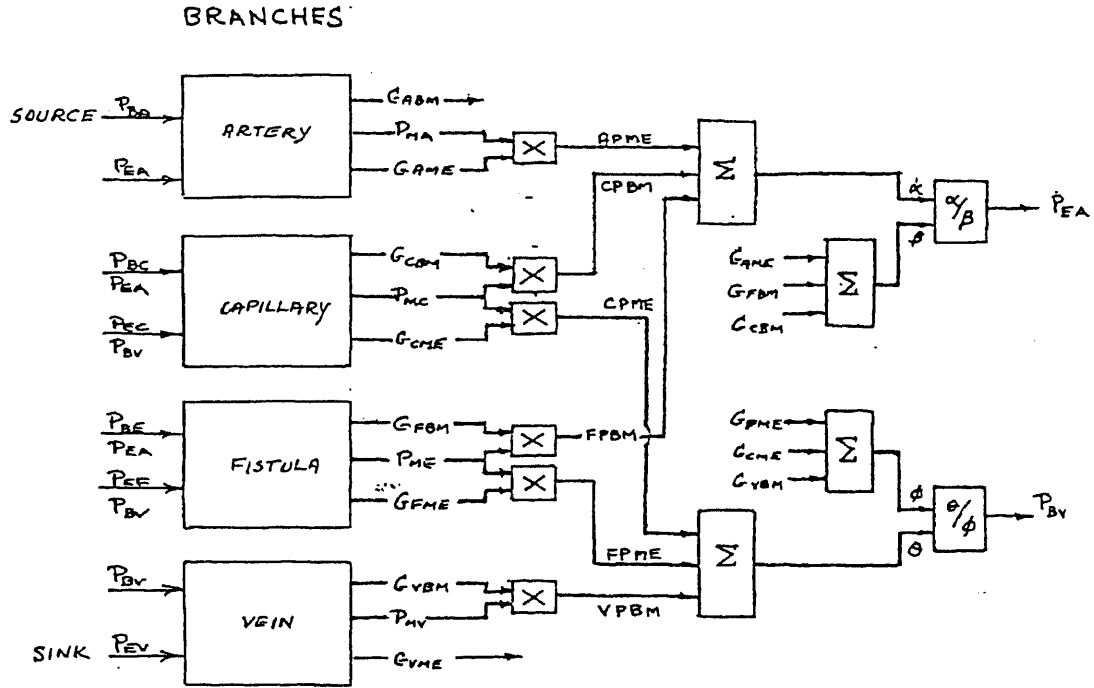
Figure 2.6 Total AVM System Block Representation

Then the branch resistance ΔR will be

$$\Delta R = \frac{\Delta P}{Q} = \frac{10.5}{50 \times 100} \approx 2*10^{-3}(mmHg - \min / ml)$$

The model also assumes that the total resistance of the AVM branch is 1/4 the resistance of the overall capillary branch. From these values and published estimates of anatomic radii (see Table 2.1), the proportionality constant K for the various branches can be evaluated in accordance with equation(2.14).

For the arterial branch:

$$K = \frac{1/(2 \cdot 10^{-3})}{0.95^4} = 614 \quad [\text{siemens/mm}^4]$$

(2). Functional relationship between radii and transmural pressure

From the radii(r) vs. transmural pressure (Ptr) curve obtained from Blesser (figure 2.7), a linearized relation around a quiescent operating point at the branch midpoint is assumed, and can be expressed as

$$r = r_0 + mPtr \quad\quad\quad\quad (2.15)$$

For the arterial branch:

At the quiescent point, assuming[7]

r =1mm   Pma = 32 mmHg

and the excursion of Pma is from 27 to 37 mmHg. Thus

$$\Delta p_{ma} = (37 - 27) = 10mmHg$$

For this pressure variation, r is also assumed[7] to vary between 0.5 and 1.5 mm or

$$\Delta r = 1mm$$

The compliant effect m would be

$$m = \frac{\Delta r}{\Delta P_{ma}} = \frac{1}{10} = 0.1$$

The intercept, r_0, can be derived by assuming[7] that at quiescence r = 1 mm and Pma = 32 mmHg

Thus, substituting into equation(2.15),

$$1 = r_0 + 0.1*32$$

or $\quad\quad\quad\quad\quad r_0 = -2.2$
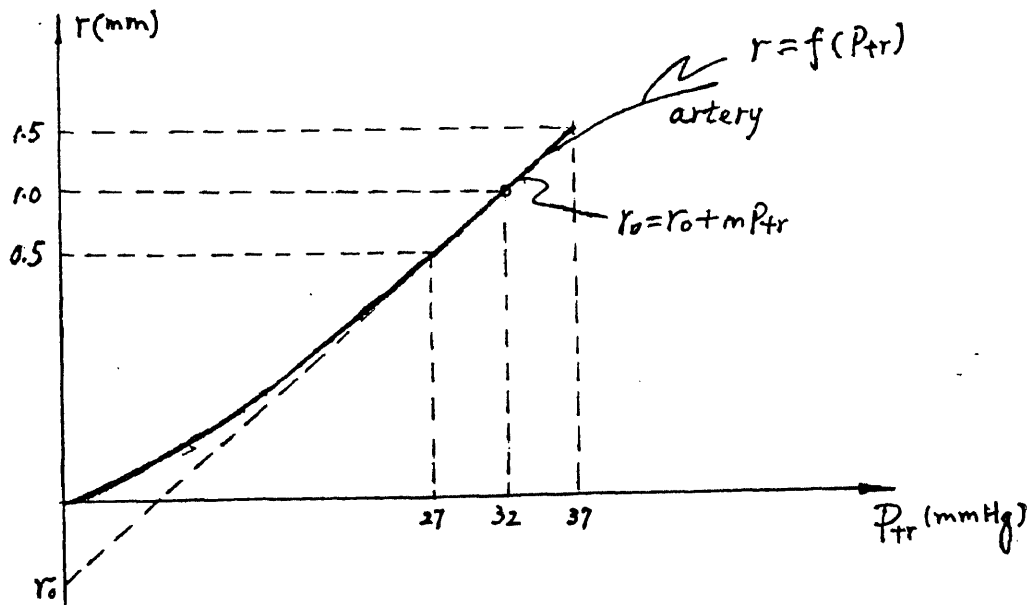
Figure 2.7 Radii-Transmural Pressure Curve

As shown in figure 2.7, r can have a negative value and still produce a physiologically meaningful relationship between radius r and transmural pressure Ptr. In the figure,

r varies between 0.5 and 1.5mm as Ptr varies between 27 and 37mmHg. Considering the compliant effect m, the values shown in the table 2.1 assume that this compliant effect (m) increases as the veins are approached.

(3). Length of branch segments:

From the definition of the conductance constant K, equation(2.14), we obtain

$$K = \frac{\pi}{8L\eta} \tag{2.16}$$

Since K has already been evaluated and the viscosity of blood (η) is a physical "constant" ($\eta = 2.6 \cdot 10^{-5} mmHg - \sec$), then, for each segment, L can be calculated by

$$L = \frac{\pi}{8K\eta} \tag{2.17}$$

For the artery:

$$L = \frac{\pi}{8 \cdot 600 \cdot 2.6 \cdot 10^{-5}} = 26 \quad [\text{mm}]$$

(4). Compliance of branches:

The compliance (C) is defined as volume change (ΔV) / pressure change (ΔP), that is

$$C = \frac{\Delta V}{\Delta P} \tag{2.18}$$

and for a tubular elements

$$\Delta V = \pi L (r_{max}^2 - r_{min}^2 \ ) \tag{2.18}$$

where $\qquad r = r_0 + mP_{tr}$

For the artery.

$$r_{max} = -2.2 + 0.1 * 37 = 1.5 \ mm$$

$$r_{min} = -2.2 + 0.1 * 27 = 0.5 \ mm$$

$$\therefore \Delta V = \pi * 2.6 * (1.5^2 - 0.5^2) = 314 \ mm^3$$

$$\Delta P = P_{max} - P_{min} = 37 - 27 = 10 \ mmHg$$

$$\therefore C_a = \frac{\Delta V}{\Delta P} = \frac{314}{10} = 31.4 \ mm^3 / mmHg$$

These parameters can be arranged in table 2.1.

Table 2.1 Values of system parameters

Tube	Seg	resist. $\times 10^3$	rad. mm	K	Pmx (avg)	m	r_o	len. mm	1/C
ART	ABM	2	.95	600	32	.1	-2.2	25	.03
	AME	2	.95	600		.1	-2.2	25	
CAP	CBM	8	.8	300	13	.12	-.76	50	.013
	CME	4	.95	300		.14	-.87	50	
AVM	FBM	1.5	1.2	300	16	.12	-.72	50	.011
	FME	1.5	1.2	300		.14	-1.04	50	
VEIN	VBM	.5	1.35	600	7	.18	.24	25	.01
	VME	.5	1.35	600		.18	.24	25	

Using all the above equations, diagrams and system parameters, the VisSim modeling software discussed in the Appendix was used to simulate the entire model. We will begin at the "SOURCE" branch.

The VisSim block diagram of the "SOURCE" is shown in figure 2.8, where block 1 is the sinusoid function generation block which has amplitude 80 and frequency 6.28. Block 2 is the limit block which has lower limit 0 and upper limit 300 and is used to limit the output signal to the specified upper and lower bound. Block 3 is a summingjunction block which performs the summation of the two input signals, one from block 2, the other from block 5. Block 4 is a gain block that produces the product of the input signal coming from the summingjunction block and the specified gain. Block 5 is an integration block which performs the integration of the signal coming from block 4; the values shown in the block represent the initial condition and the block ID. Block 6 is also a gain block, which performs a feed back function from block 5 to block 3. The combination of these blocks from "A" to "B" performs the solution of the first order differential equation which is similar with that shown in the appendix. The differential equation of the source branch can be derived from figer 2.8 and is shown in equation(2.20).

$$\dot{Y}(t) + \frac{3}{4}Y(t) - 60\sin(t) = 0 \qquad (2.20)$$

$$8\sin(t) + 14 + Y(t) = P_{ba}(t) \qquad (2.21)$$

Figure 2.8 The VisSim Block Diagram of "SOURCE" Branch

Block 7 & block 8 are similar to block 1 & block 2 used as a function generator. Block 9 is a constant block which has the constant value of 14. With the summing junction block(block 10), the final result Pba is obtained from the summation of the constant, sinusoid function and y(t) which is derived from the differential equation. Thus from "B" to "C", the equation can be derived and shown in equation(2.21). The curve plotted in the plot block shows the simulation result with the output ranging from 35 to 50 mmHg. Figure 2.9 shows the VisSim block diagram of the two node equations which are represented in equations(2.12) & (2.13). Variable blocks "APME", "CPBM", "FPBM" and "VPBM" are the result of the products of vessel pressure and conductance of each branch in figure 2.10 to figure 2.13. For instance, "APME" is the result of the product of Pma and Game, which is shown in figure 2.10. Block 12 & block 13 are the divide(/) blocks, it makes the input 1 divided by r. In the figure, the five compound blocks on the left side represent the artery, capillary, fistula and vein branches as well as the input source. figure 2.10 to figure 2.13 shows the VisSim diagram of each vessel branch. The artery branch is shown in figure 2.10, where the whole block diagram can be divided into several sections. The diagram from "A" to "B" represents the simulation of the differential equation(2.8). Pba is the known input source, Pea, Pma are the distal and central feeding artery pressures. Blocks 1,2,3 & 4 are the
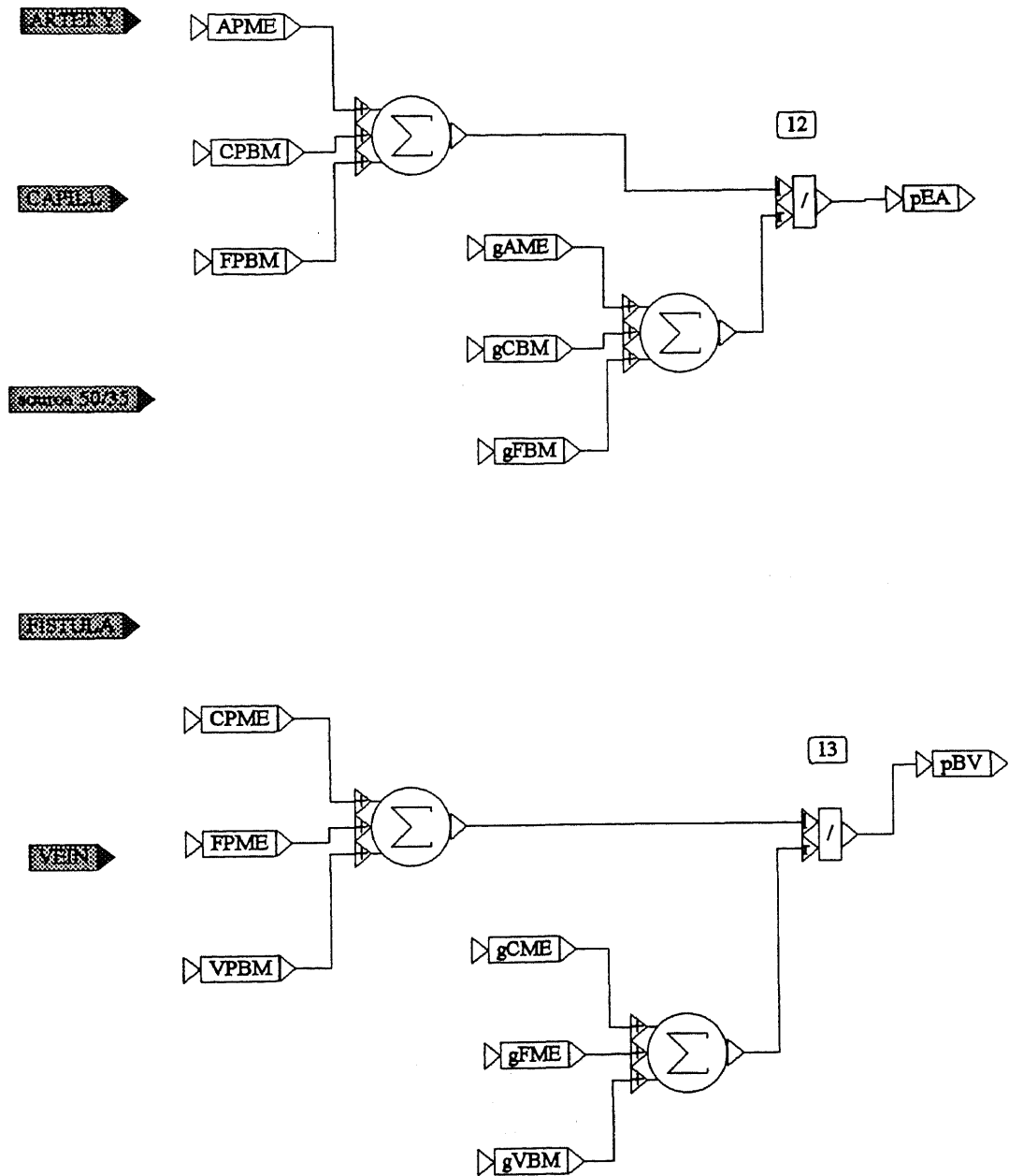
VisSim-Diagram1:source & 4 branches

Figure 2.9 The VisSim Block Diagram
of the Two Node Equations

VisSim-Diagram1:source & 4 branches.ARTERY
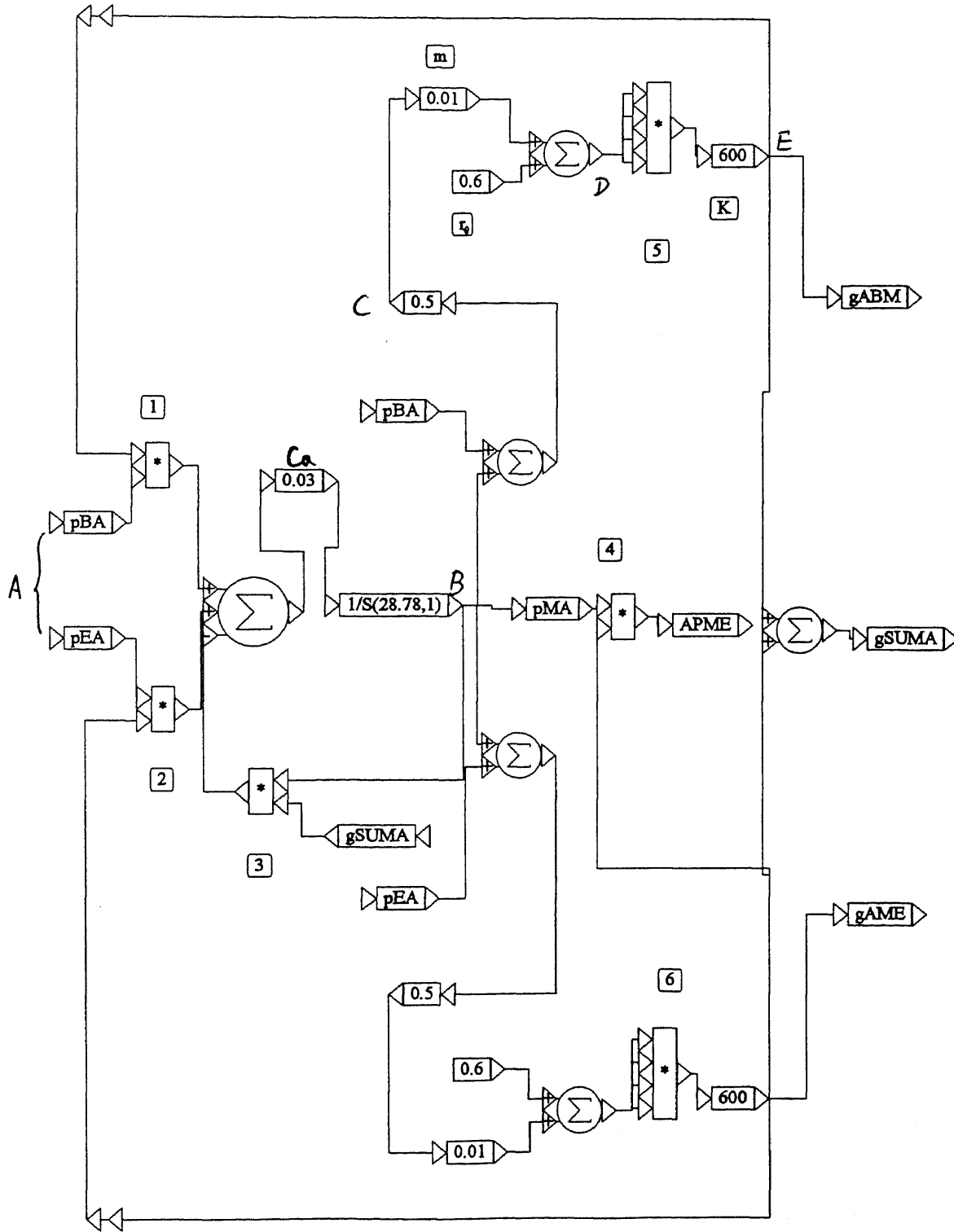
Figure 2.10 The VisSim Block Diagram
of the Artery Branch

multiply(*) blocks. "B" to "C" simulates the transmural pressure Ptr expressed in equation(2.7), "C" to "D" represents the radii-transmural function expressed by equation(2.15). Point "D" is the output of vessel radius(r). Block 5 is also a multiply block, and acts to multiply the input(r) four times. That is to say, this block produces the fourth power of the radius(r^4). After that, multiplied by a constant(K), the vessel proximal conductance Gabm which is expressed in equation(2.14) was derived. The vessel distal conductance Game was derived in the same way. The VisSim block diagram of capillary branch, fistula-like AVM branch and draining vein branch can also be obtained using a similar method and are shown in figure 2.11-2.13.

In the fistula branch shown in figure 2.11, two "fist botm" blocks are used to simulate the proximal and/or distal cutting of the AVM. figure 2.15 is the resulting display, where any four parameters can be displayed simultaneously. Here we selected Pea, Pmc, Pmf, and Pmv, and the two "button" blocks located on the left lower corner denote the fistula proximal and distal switch, respectively, to simulate the AVM occlusion. The "Source and 4 branches" block is treated as a compound block. The VisSim program allows you to use the "mouse" to point to the top of the compound block, then double click to get into the second stage of the block diagram that is represented by this compound block. For example, in figure
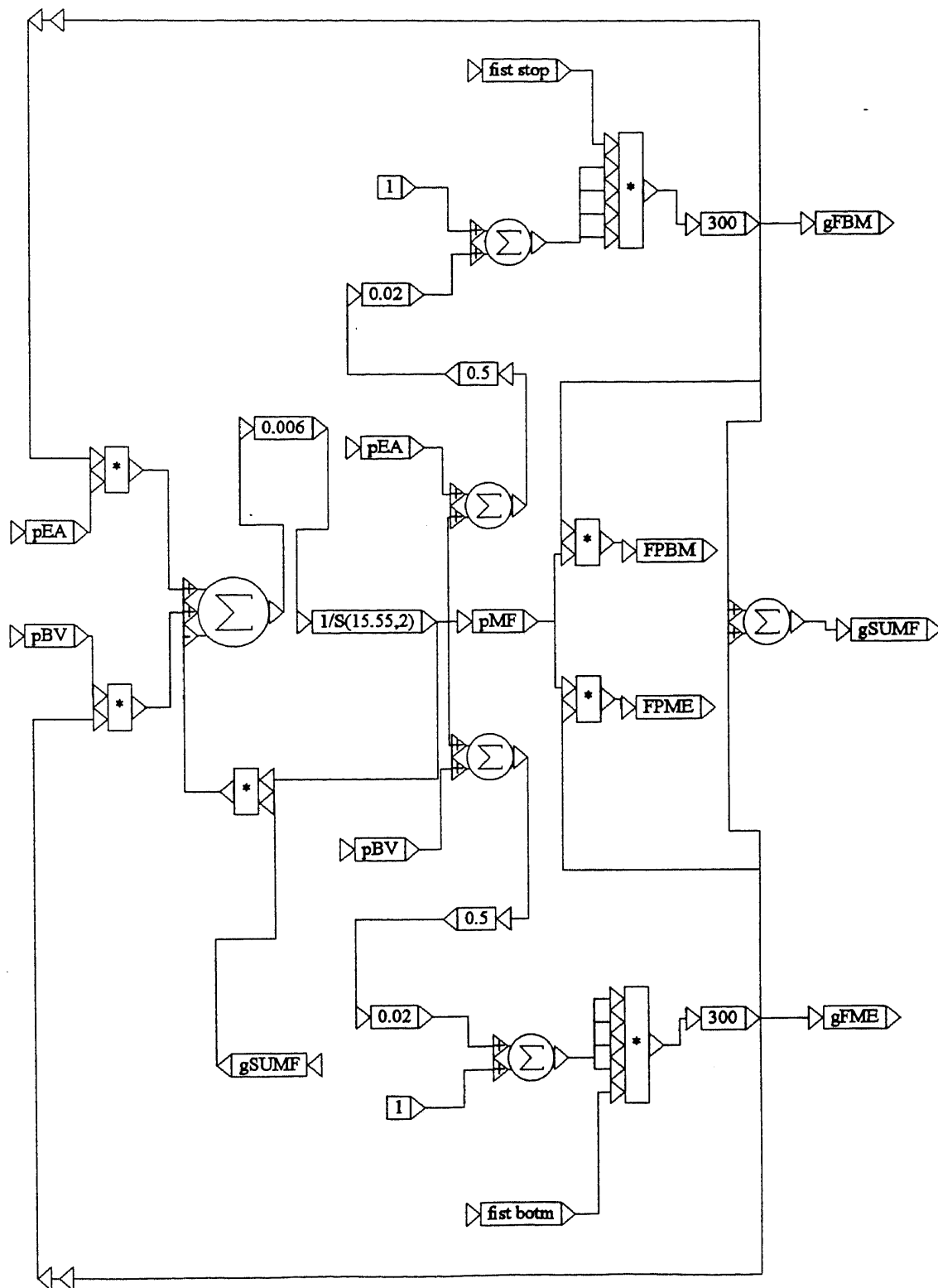
Figure 2.11 The VisSim Block Diagram of Fistula Branch
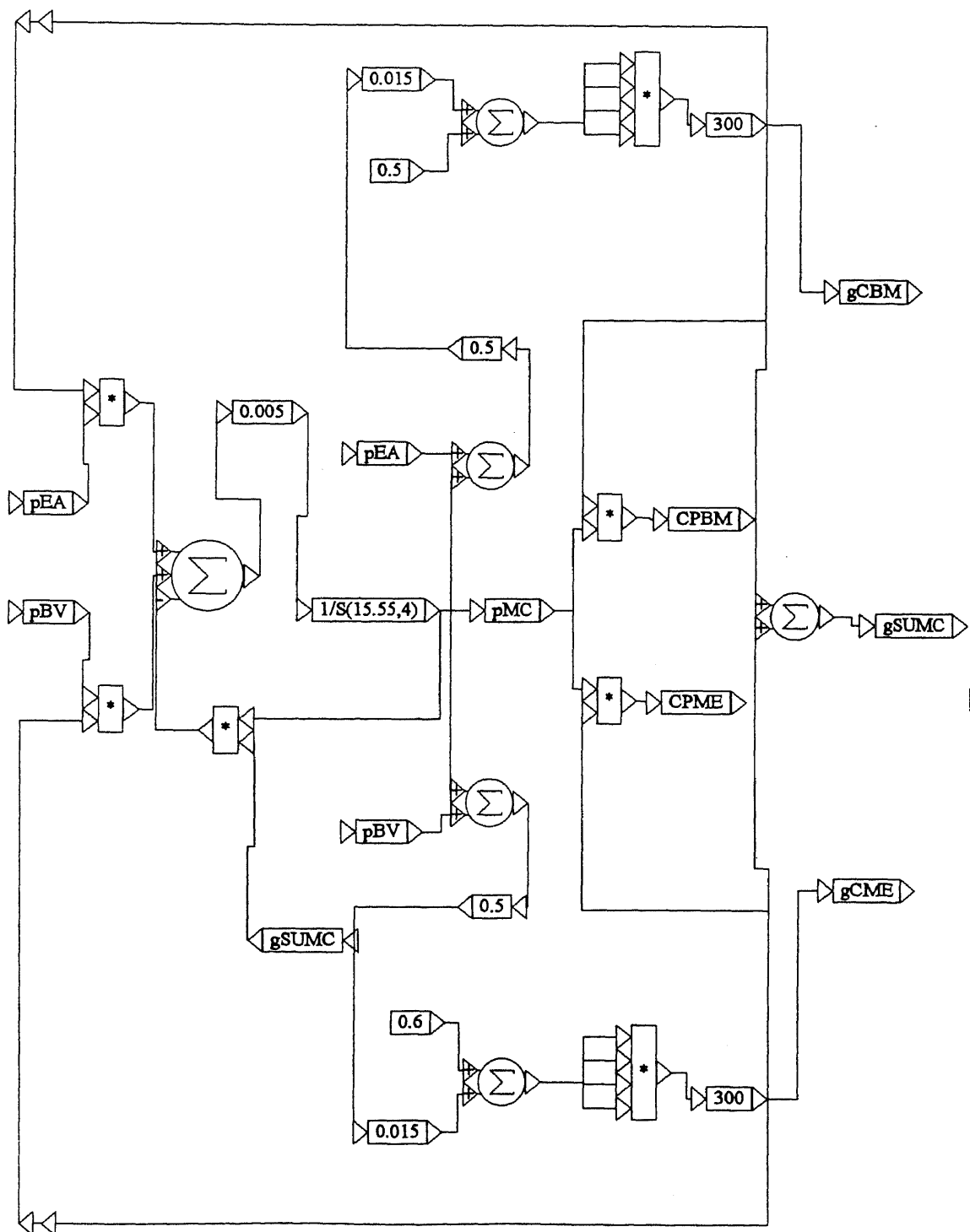
Figure 2.12 The VisSim Block Diagram of Capillary Branch
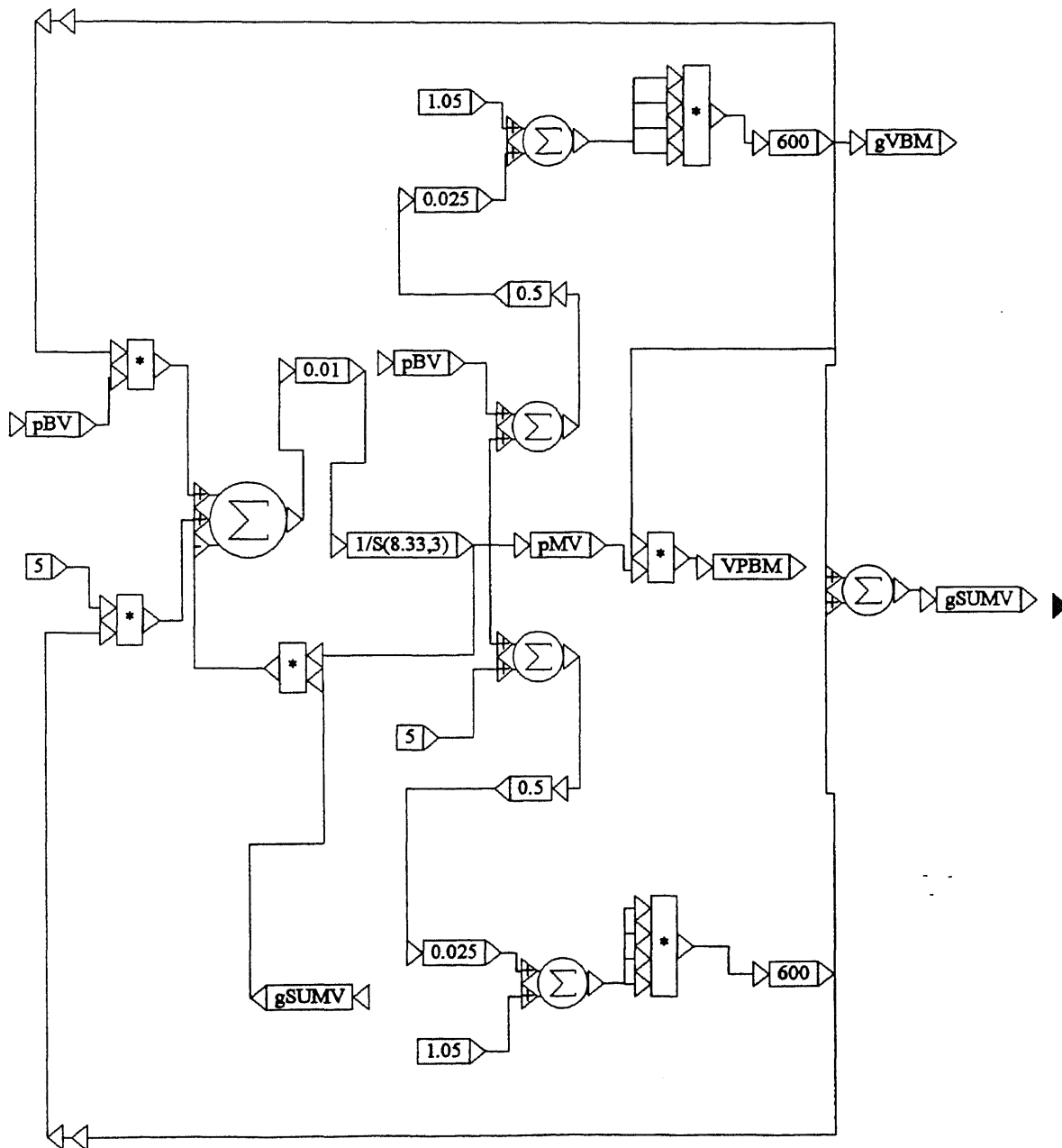
Figure 2.13 The VisSim Block Diagram of Vein Branch

A: The Compound Block of "SOURCE 50/35"
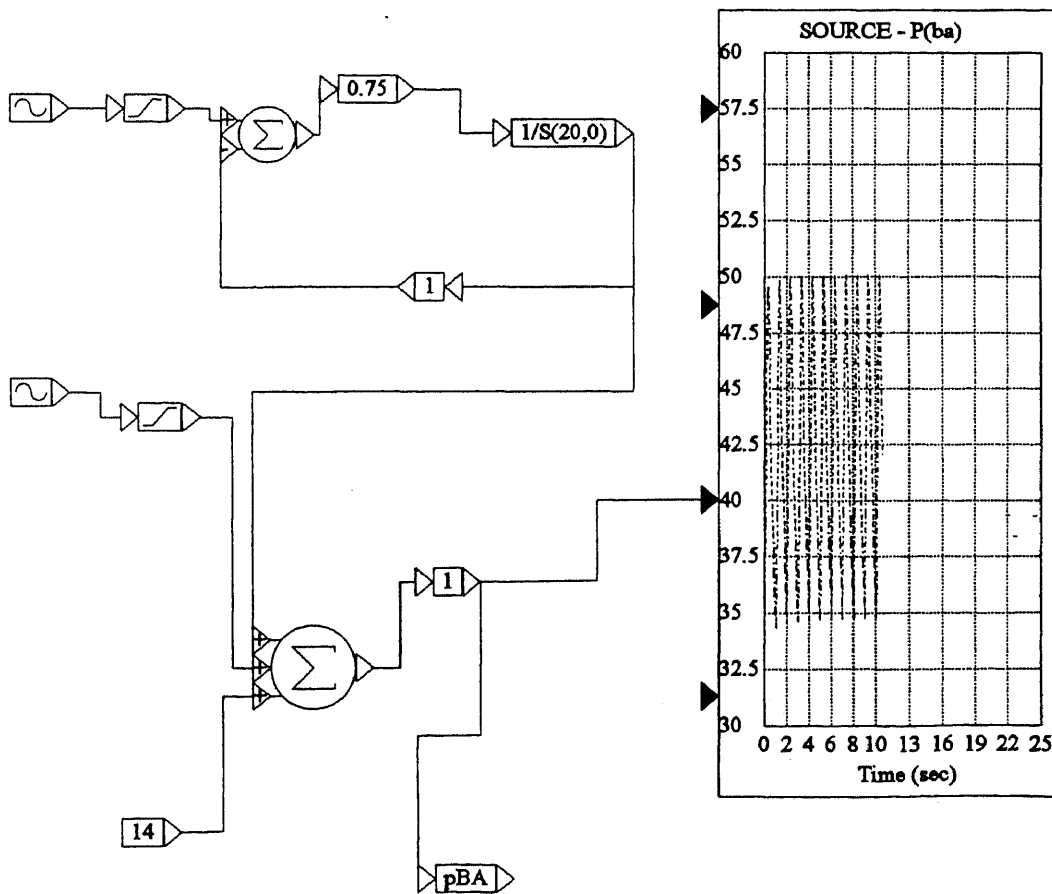
B: The Second Stage of the "SOURCE 50/35" Block Diagram

Figure 2.14   The Diagram of a Compound Block
and Its Second Stage Block Diagram

VisSim-avm83093.vsm
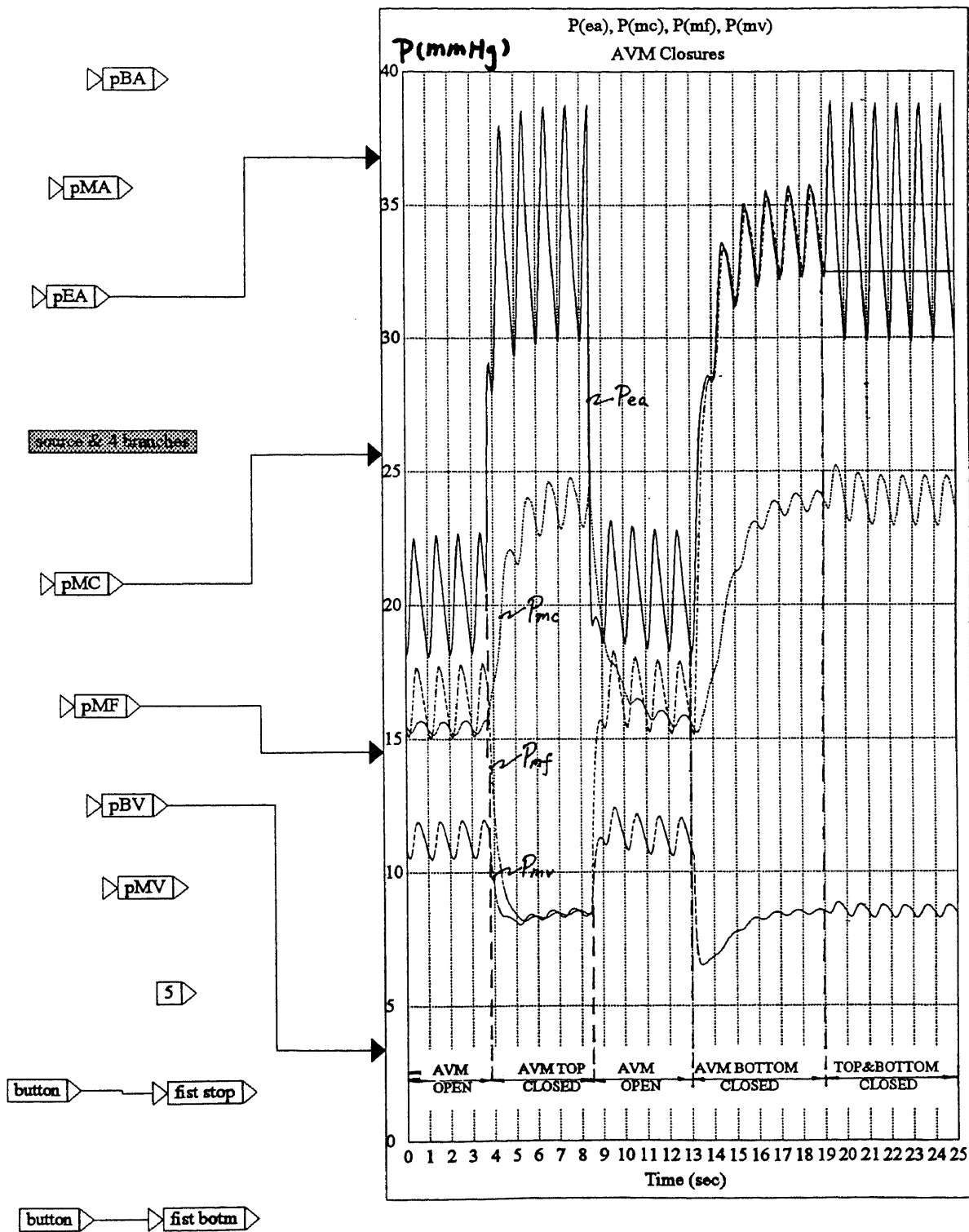
Figure 2.15 The Resulting Display Diagram

VisSim-avm83093.vsm
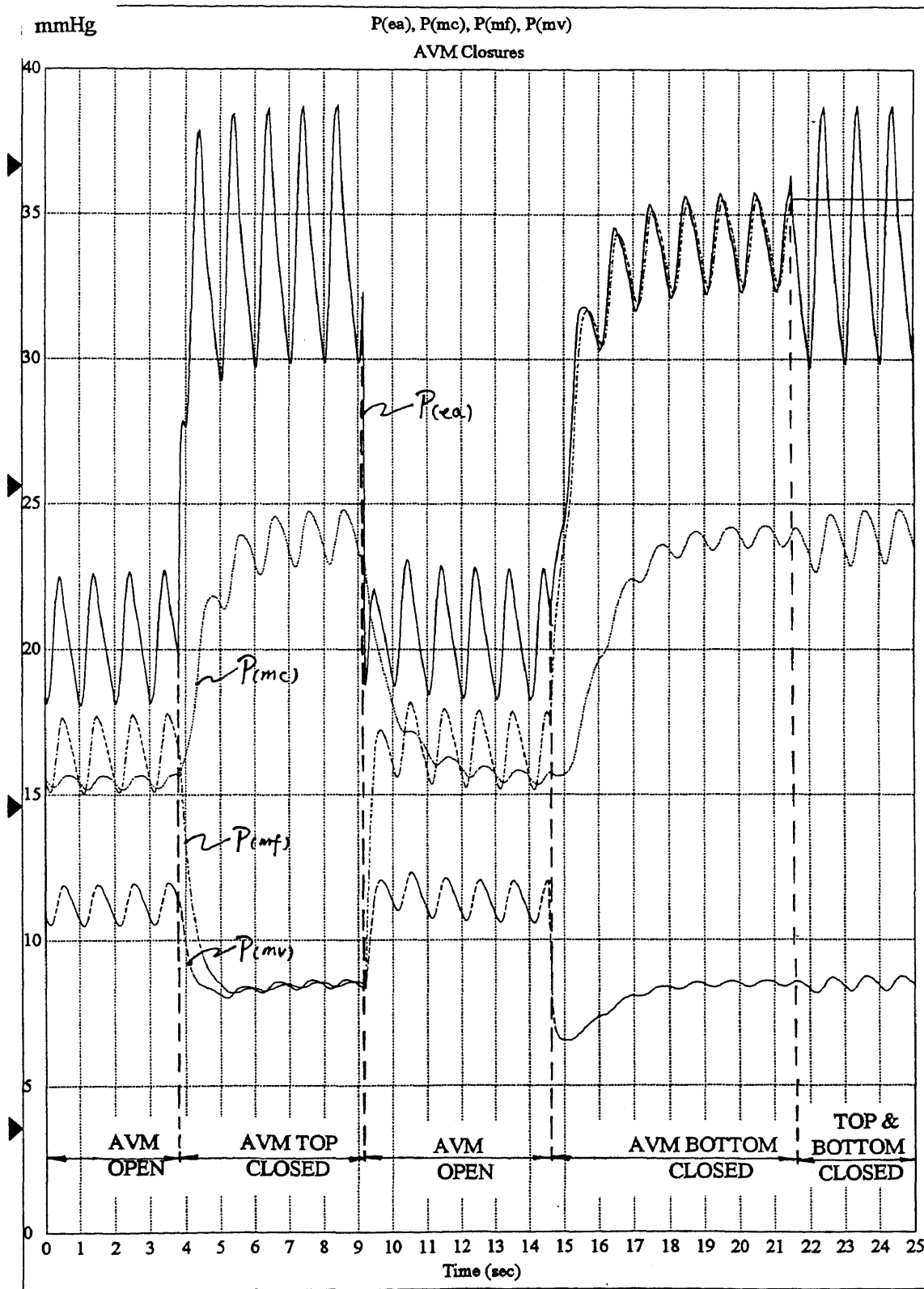
Figure 2.16 The Simulation Result with AVM Occlusion

compound block is double clicked, the second stage of the diagram---source diagram appears as shown in the lower part of figure 2.14. Thus for the compound block of "source and 4 branches" in figure 2.15, the second stage diagram of this block figure 2.8 will appear after it is double clicked, and any one of the compound blocks in that diagram can be examined.

The simulation result with AVM occlusion is shown in figure 2.16. In the figure, the four pressure curves represent the distal arterial pressure(Pea), capillary pressure(Pmc), fistula pressure(Pmf) and the draining vein pressure(Pmv) which are plotted against time. The simulation results show that the pressure response is dependent on the site of AVM occlusion. When the AVM is blocked proximally, the capillary pressure Pmc is increased to approximately 25 mmHg which may result in brain swelling and edema. Fistula pressure rapidly falls following proximal occlusion. This is in contrast to a marked rise in fistula pressure to near arterial levels with distal occlusion, which also may be the reason for the brain swelling and hemorrhage.

2.3 The Principle of Autoregulation

We will now discuss the principle of autoregulation. Cerebral autoregulation is a physiological regulatory mechanism that maintains a constant flow over a wide range of cerebral perfusion pressure. It operates on whatever blood flow is present in the brain, trying to maintain flow

constant by dilation of resistance vessels when the blood pressure falls and constriction when the pressure rises. Let us consider the equation

$$CBF = \frac{CPP}{CVR}$$ (2.22)

where CBF is the cerebral blood flow, CPP the cerebral perfusion pressure and CVR the cerebrovascular resistance. It is seen that completely effective autoregulation implies that CBF remains constant and that CVR changes proportionally to changes in CPP, that is, if CPP increases or decreases, CVR will also increase or decrease to counterbalance the change of CPP so that CBF is maintained constant. On the other hand, completely abolished autoregulation implies that CBF changes proportionally to changes in CPP and that CVR remains constant (or even inversely proportional to changes in CPP). One hypothesis for the autoregulation mechanism[4] called the myogenic hypothesis, suggests that the smooth muscle of the cerebral vessels is responsive to changes in perfusion pressure, and that this is predominant in the smaller resistance vessels[4][7][8]. Thus, our model simulates autoregulation by means of arterial dilation and constriction in the precapillary branch: Vessels dilate with falling perfusion pressure and they constrict with rising perfusion pressure.

CHAPTER 3

MODEL DEVELOPMENT

In order to better understand the reasons for brain swelling
and hemorrhage after AVM occlusion, several factors that may
affect the hemodynamic response following AVM occlusion were
considered in my thesis work. They are: (1) different
degrees of autoregulation mechanism failure; (2) sympathetic
nervous system dysfunction and (3) increased intracranial
pressure.

3.1 Different Degrees of Autoregulation Failure

Based on the principle of autoregulation discussed in
chapter 2 , a curve of resistance (CVR) vs. cerebral
perfusion pressure (CPP)[5] which satisfies the
autoregulation mechanism is shown in figure 3.1, where CVR
represents the vessel resistance of the small arteries,
arterioles and capillaries. For the purpose of
autoregulation over the range from 60 to 130 mmHg of
cerebral perfusion pressure(CPP), CVRA must vary between
0.065 and 0.155 mmHg-min./ml. When CPP drops below 60 mmHg,
autoregulation fails. In our AVM model, we separated the
small arteries and arterioles as well as capillaries. In
order to make the model simpler, we consider only one branch
having the autoregulation behavior, that is, the
precapillary branch. Thus several parameters in the existing

autoregulation curve need to be modified so that the new autoregulation curve will match the existing AVM model. figure 3.2 shows the modified autoregulation curve, where CVR must vary between CVRB and CVRM when CPP ranges from 5 to 55 mmHg. This CPP has a different meaning from the original CPP shown in figure 3.1, where the former represents the pressure difference between mean arterial pressure and intracranial pressure, and the modified variable involves only the mean precapillary pressure. Therefore, the range of this CPP is much smaller. When CPP drops below 5 mmHg, autoregulation fails. Mathematically, we can express this as

$$CVR = \begin{cases} CVRM - \dfrac{CVRD}{1+(CPP/NCPP)} \ , & CPP/NCPP >= CL \\[3em] CVRB\,(0.15\,NCPP/CPP) \ , & CPP/NCPP < CL \end{cases} \qquad (3.1)$$

Here NCPP is normal perfusion pressure and CL is the lowest limit value of CPP. CVRB, CVRM and CVRD are the three parameters that can be regulated to represent the different degrees of autoregulation. A set of these examples are listed in table 3.1. The simulation block diagram of equation(3.1) is illustrated in figure 3.3. Figure 3.4 shows the simulation result of different degrees of autoregulation

VisSim-automao4.vsm
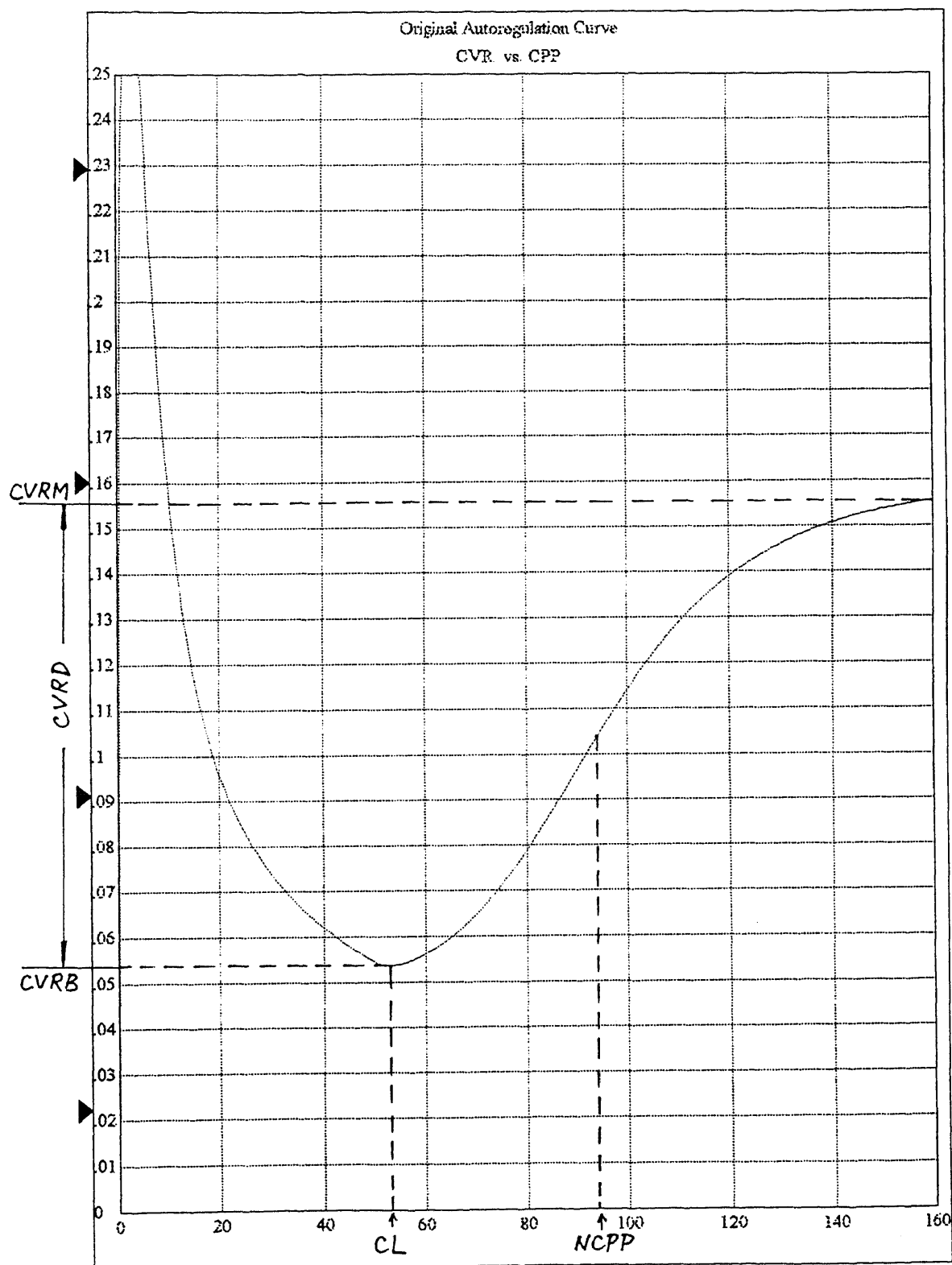
Figure 3.1 Original Autoregulation Curve

VisSim-automao3.vsm
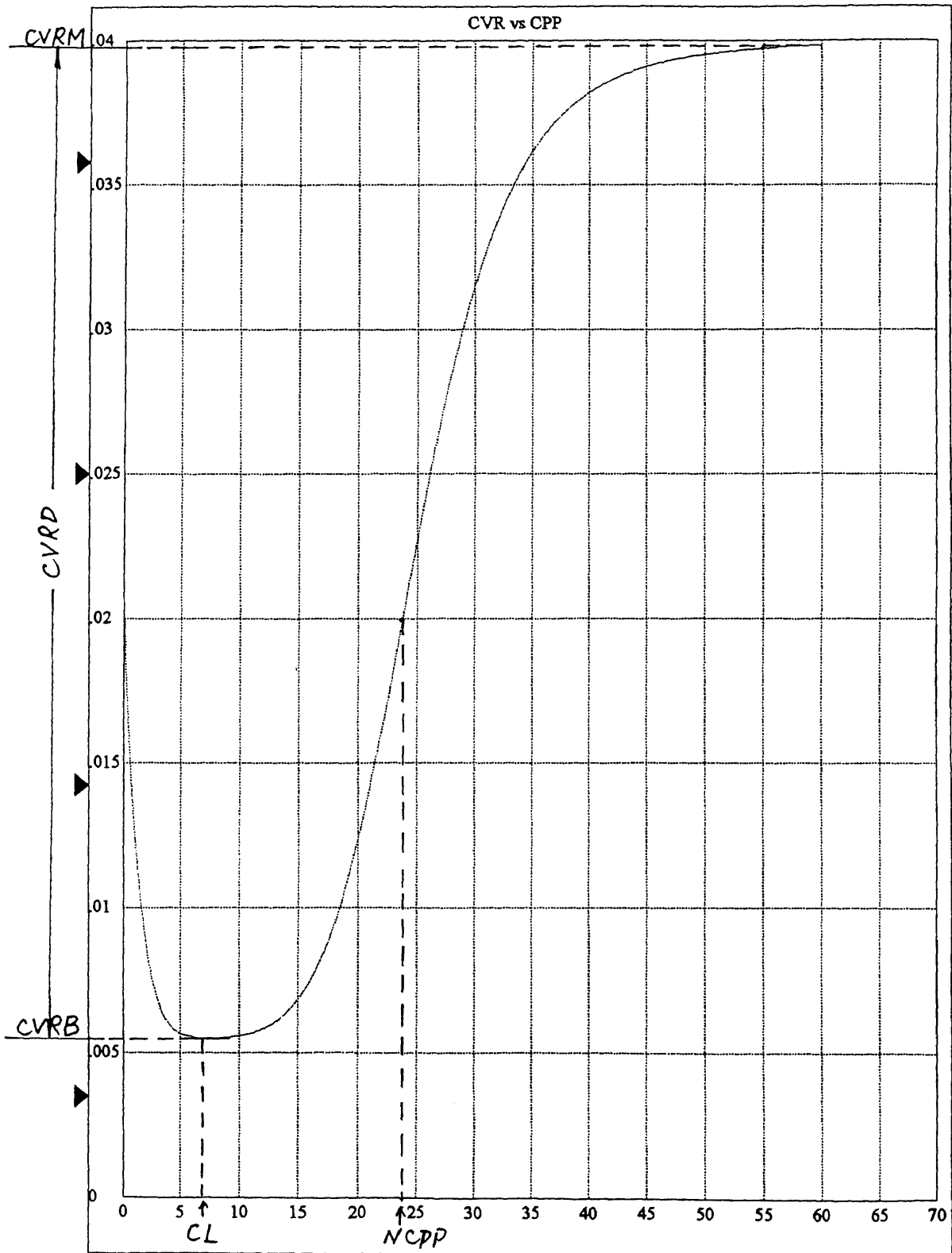
Figure 3.2 Modified Autoregulation Curve

VisSim-automao3.vsm
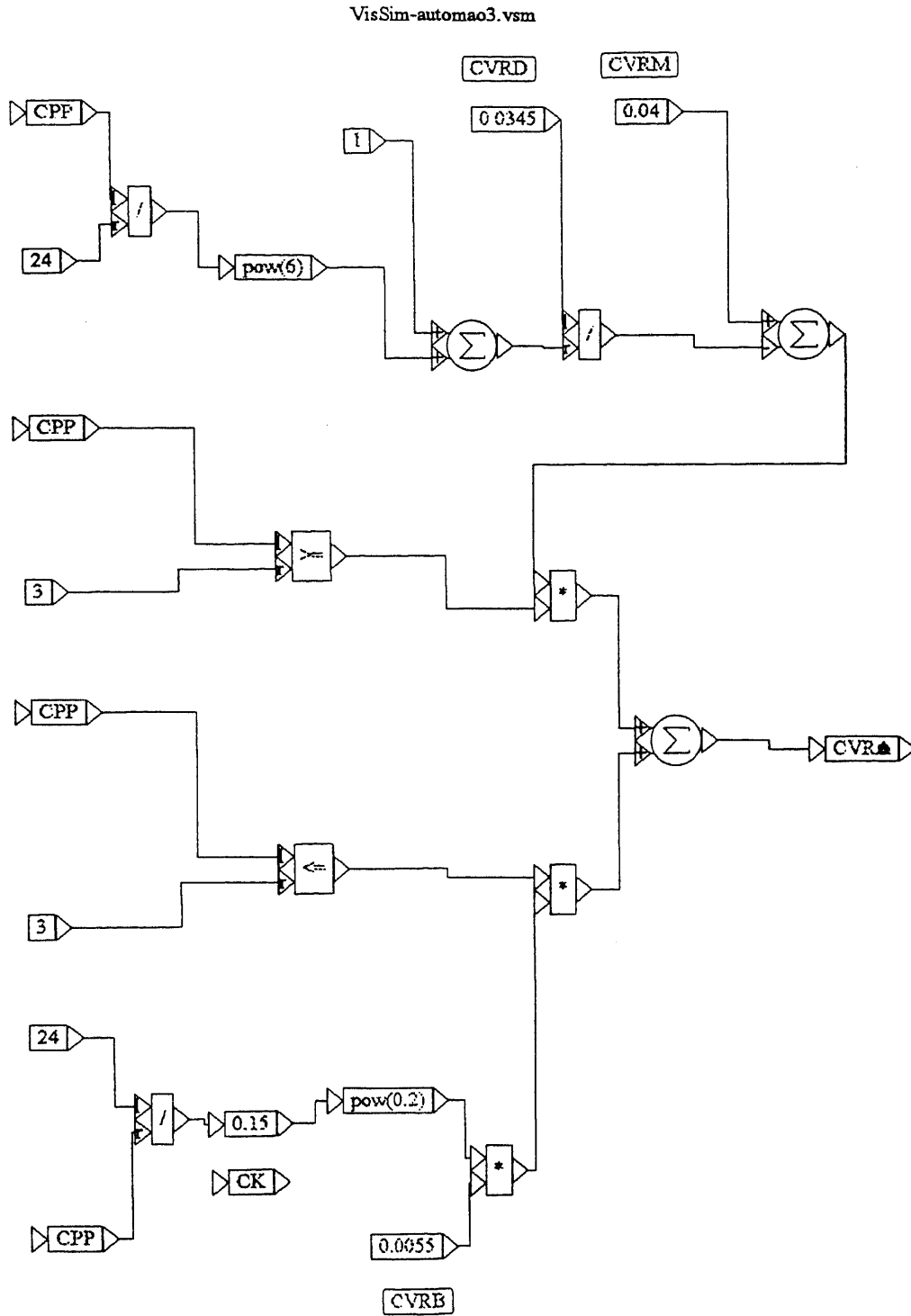
Figure 3.3 The VisSim Block Diagram
of Autoregulation Function
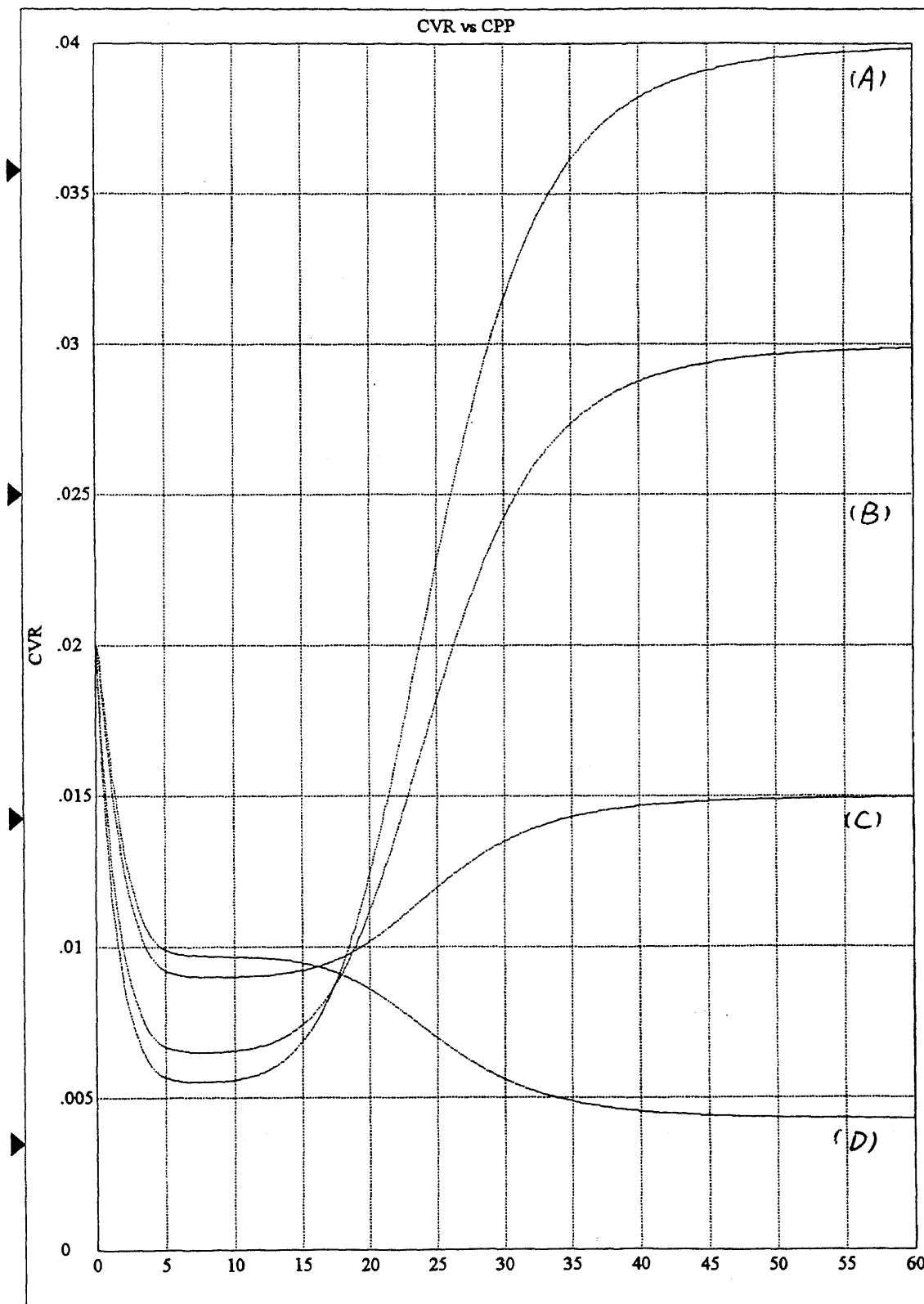
Figure 3.4 Different Degrees of Autoregulation Curve

Table 3.1 Different parameters of autoregulation

	CVRB	CVRM	CVRD
CURVE A	0.0055	0.04	0.0345
CURVE B	0.0065	0.03	0.0235
CURVE C	0.009	0.015	0.006
CURVE D	0.0096	0.0043	-0.0054

marked with A,B,C and D, which corresponds to the different sets of parameters shown in table 3.1. Note that curve A has the deepest degree of autoregulation and curve D has the shallowest. To incorporate these curves into our current model, the Gcbm, capillary proximal conductance will be replaced by 1/CVR which changes inversely proportional to the change of perfusion pressure. The autoregulation section in the VisSim diagram of the capillary branch will appear as a compound block designated as "AUTOCAPL" as shown in figure 3.5. At present, the autoregulation mechanism has only been included in the capillary branch, with the other three branches remaining unchanged. This new AVM system with the autoregulation mechanism is simulated on a 486-PC using the same VisSim graphical modeling program as the original model.
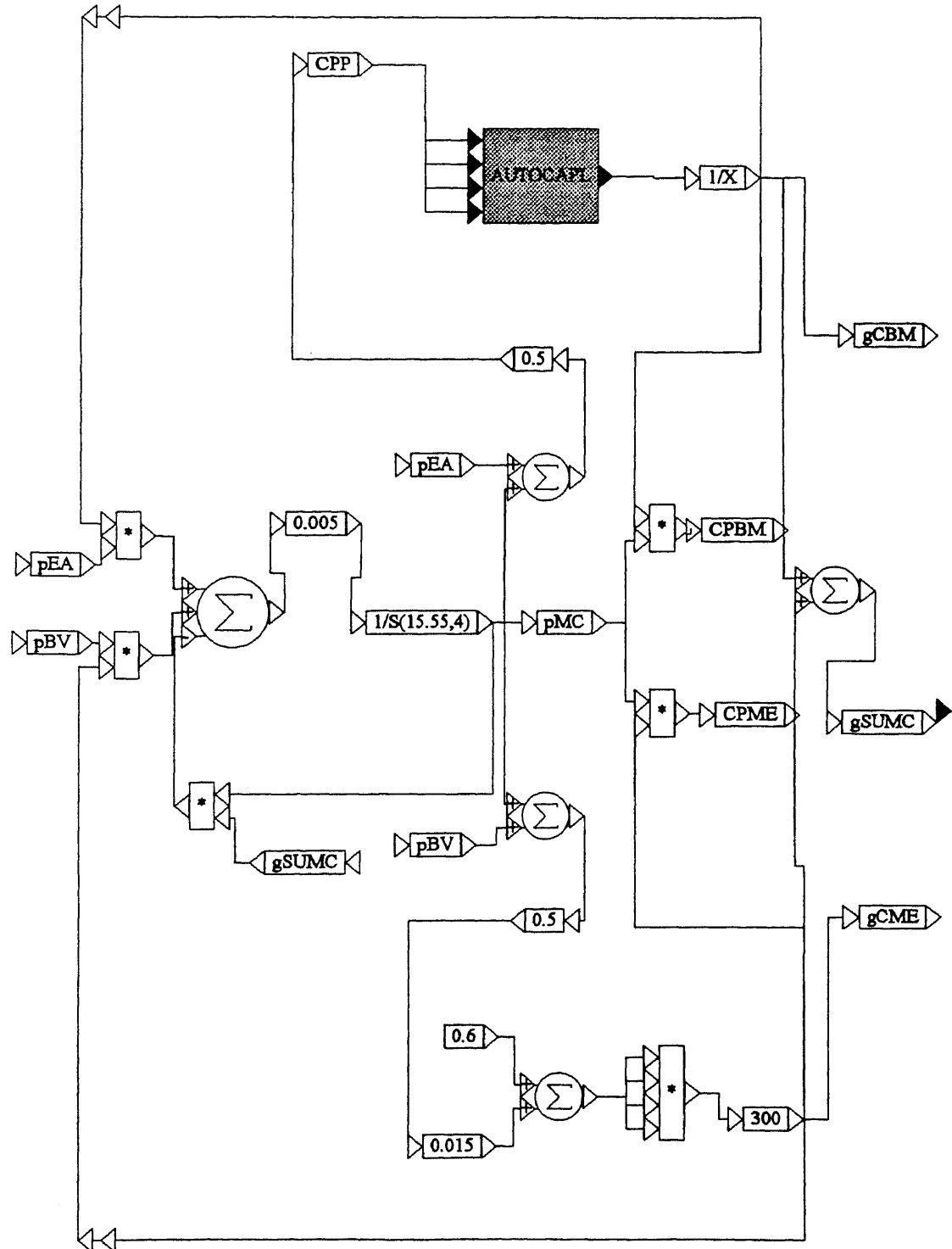
Figure 3.5 The Simulation Diagram of Capillary Branch with Autoregulation of AVM System

3.2 Sympathetic Nervous System Dysfunction

The exact role of the nervous system in cerebral hemodynamics is still a matter of discussion among physiologists. Some authors think that the neurogenic mechanism has scant importance in the control of cerebral vessels[19]. Others lay particular stress on the role that nerves might play in the regulation of CBF and cerebral blood volume(CBV)[4][8][13][14]. Some recent experimental findings, however, appear to demonstrate that at least two systems of nerve fibers operate on cerebral vessels, one is the sympathetic adrenergic vasoconstrictory system coming from the superior cervical ganglion and the stellate ganglion, the other is the parasympathetic vasodilatory system which distributes from the seventh cranial nerve and from the sphenopalatine ganglion[4][8]. The innervation density is greatest in large cerebral vessels at the base of the brain and sparser in more distal and intraparenchymal arteries[4]. In order to investigate the action of the sympathetic nervous system on the cerebral hemodynamics following AVM occlusion, we constructed an additional branch(called the sympathetic branch) which represents the vessels which come from the carotid artery and go into the feeding artery as shown in figure 3.6. This branch is assumed to perform the following function: The sympathetic nervous system action causes the vessel caliber to decrease or pressure to drop from the carotid artery to the feeding artery.
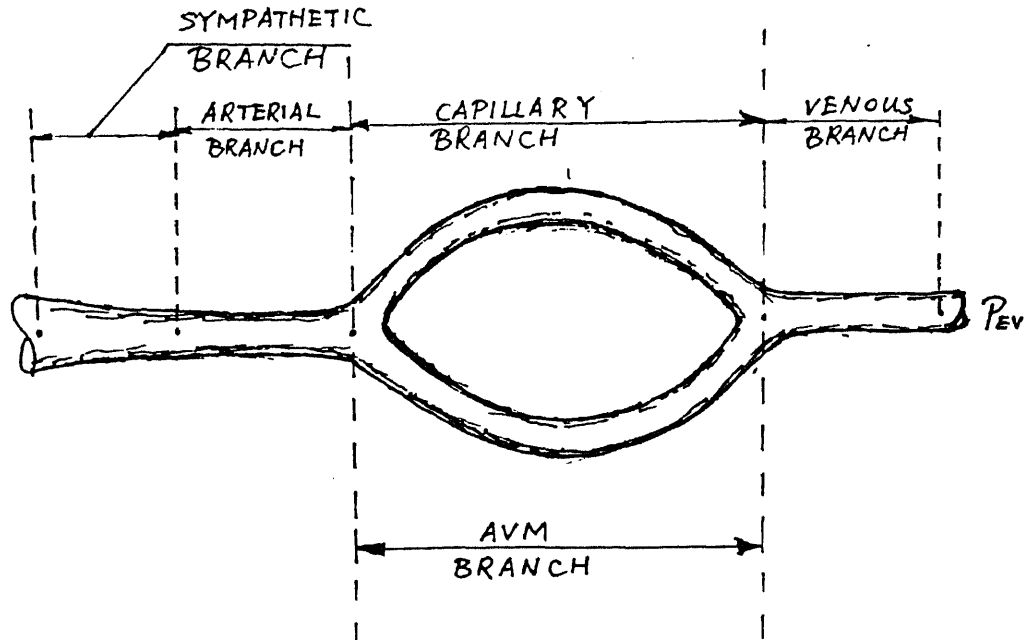
Figure 3.6 AVM System with Sympathetic Branch

The pressure drop in this branch is from 120/80 mmHg at the branch entrance to 50/35 mmHg at the branch exit and this pressure drop is assumed to be the result of vessel caliber decrease and normal sympathetic nervous system action. For simplicity during our first stage of model construction, we neglected the parasympathetic nervous system action and only considered the sympathetic stimulation and denervation. The electrical model of this branch can be constructed in a similar way as for the other four branches, that is, it can be modeled with two resistors and a capacitor represented in figure 3.7. In this model, the vessel conductance G is assumed to be constant during sympathetic denervation and changes in synchrony during normal sympathetic action.
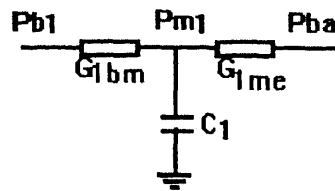
Figure 3.7 The Electrical Equivalent of Sympathetic Branch

The simulation diagram of vessel conductance G and the results are shown in figure 3.8 & figure 3.9. Figure 3.8 is the simulation diagram of vessel conductance. The "Button" block represents the switching of sympathetic nervous system action or denervation. This value can be either "1" or "0". The sinusoid block here is used to generate a sinusoidal wave that ranges from -1 to 1. The "merge" block examines the value of the "button"; if the "button" = 1, it uses the sinusoid as the output, otherwise the constant "1" will be the output. The "Sign" block determines the sign of its input signal; if its input<0, then its output is "-1", if its input>0, then its output is "1", else it outputs "0". Therefore, this block can be used to produce a square wave from a sinusoidal wave that comes from the "merge" block when the "button" equals to "1". The output range of the square wave can be regulated by changing the parameters X1, Y1 and X2, Y2 so that, when "sign" outputs "1", G1bm will be equal to (X1+Y1), G1me will be (X2+Y2); otherwise G1bm will be(-X1+Y1),G1me will be (-X2+Y2). Figure 3.9 is the simulation results of G1bm G1me, where the top curve
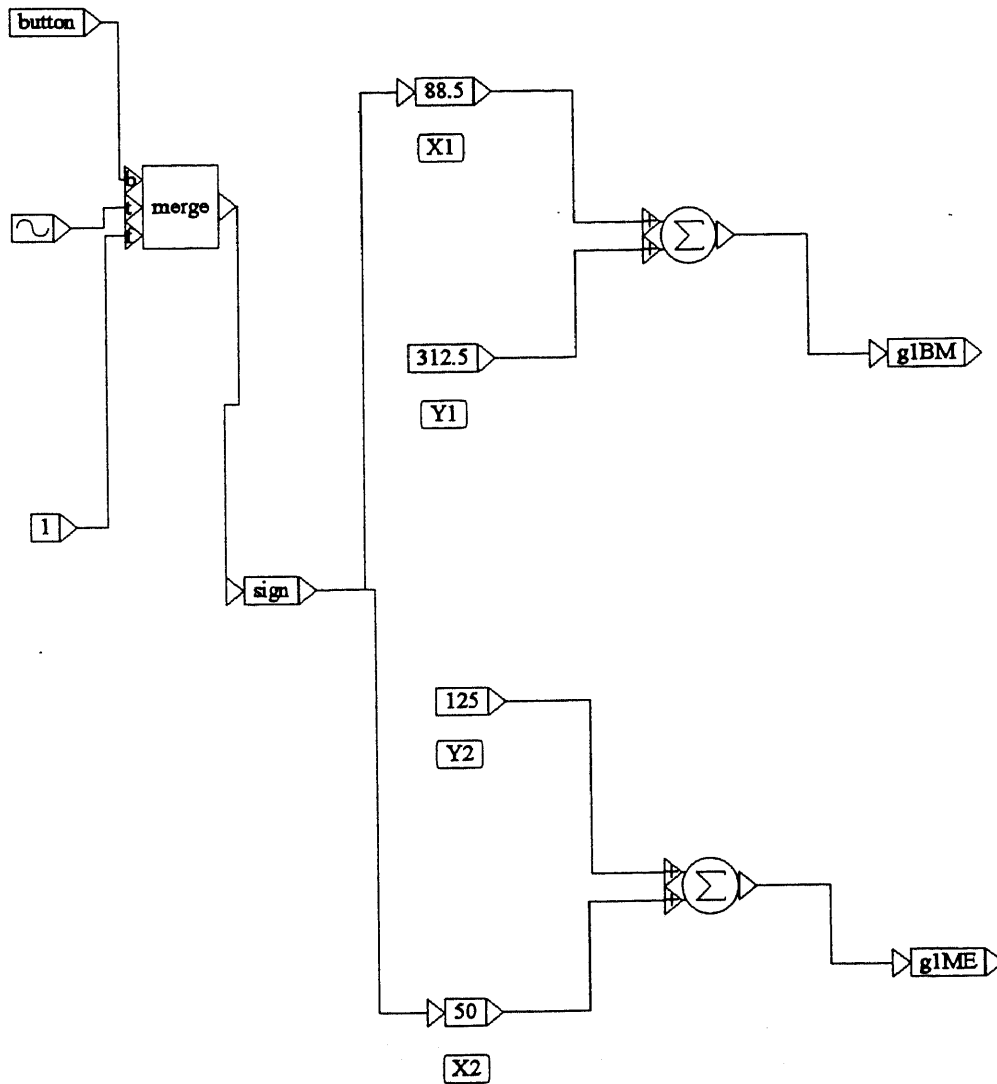
Figure 3.8 The VisSim Block Diagram of the Vessel Conductance G
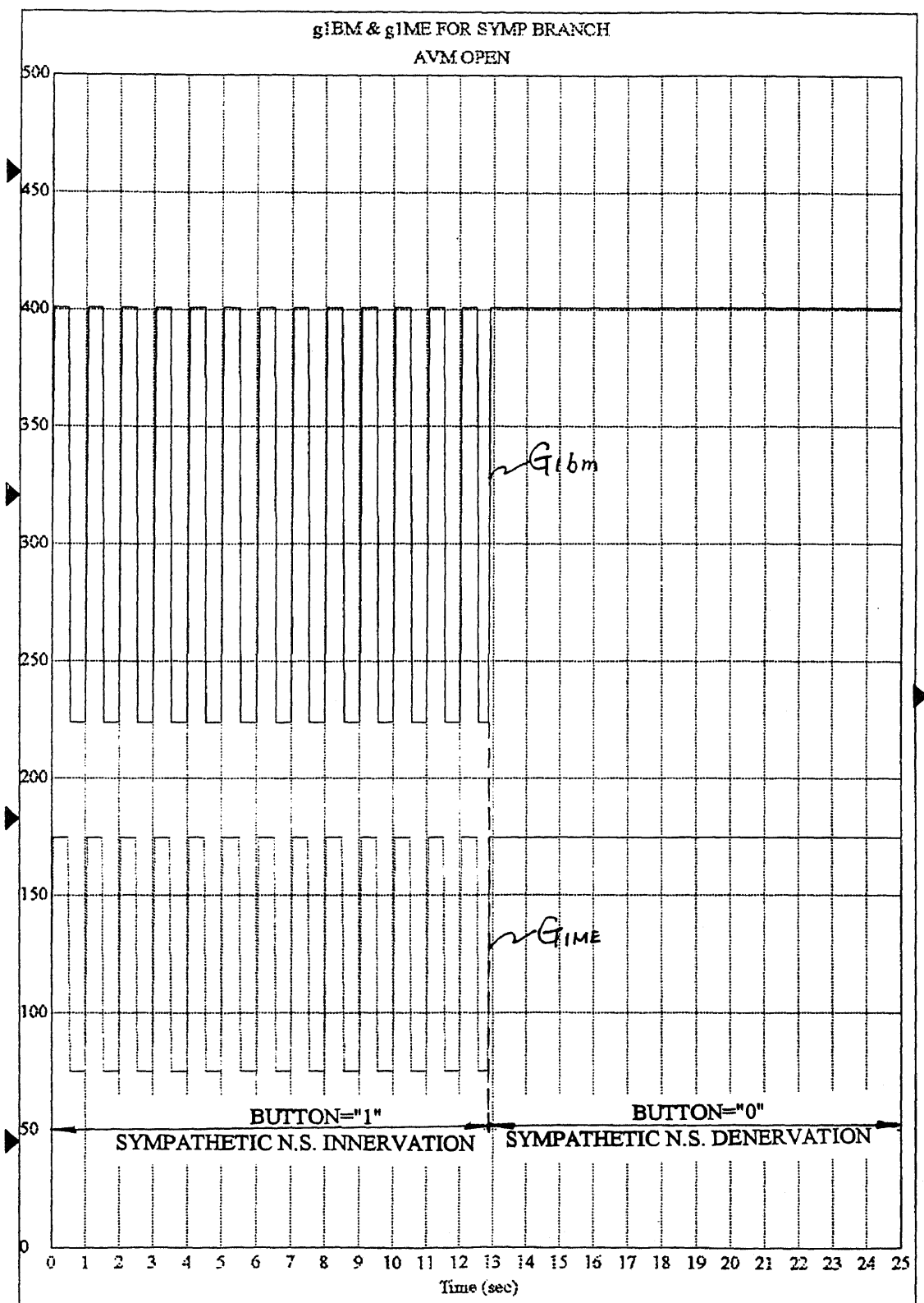
Figure 3.9 The Simulation Results of
The Conductance G1bm & G1me

is G1bm, and the lower one is G1me. The left side represents sympathetic nervous system innervation and the right side sympathetic nervous system denervation. The parameters of the other branches can be evaluated in a similar way as the original model. Thus , the complete model can be derived by connecting this branch to the front of the feeding artery branch of the original model as shown in figure 3.10.
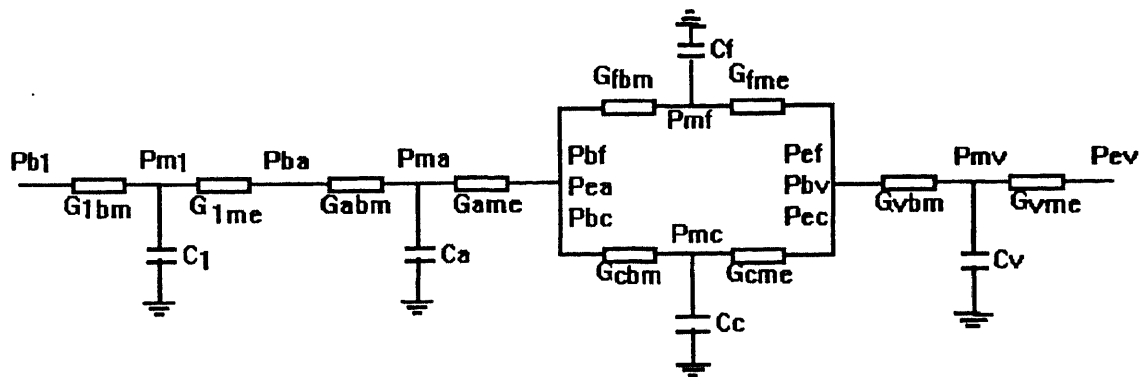
Figure 3.10 The Electrical Equivalent of
AVM System with Sympathetic Branch

In this model, we neglected the autoregulation function which existed in the proximal part of the capillary branch. To make the system solvable, two additional equations are needed for the parameters Pm1 and Pba(assume Pb1 is a known pressure source of 120/80 mmHg). The equations are:

$$(P_{B1} - P_{M1})G_{1BM} = C_1 \dot{P}_{M1} + (P_{M1} - P_{BA})G_{1MB} \qquad (3.2)$$

or $\qquad P_{B1}G_{1BM} + P_{BA}G_{1MB} = C_1 \dot{P}_{M1} + P_{M1}(G_{1BM} + G_{1MB})$

$$G_{1MB}(P_{M1} - P_{BA}) = G_{ABM}(P_{BA} - P_{MA}) \qquad (3.3)$$

or $\qquad P_{BA} = \dfrac{G_{1MB}P_{M1} + G_{ABM}P_{MA}}{G_{1MB} + G_{ABM}}$

The simulation block diagrams of equation(3.2) and (3.3) can be derived in a similar way as shown in the appendix and are illustrated in figure 3.11. Together with the original equations, the present model was also simulated with the same VisSim software and some qualitative results were derived which will be discussed in Chapter 4.

3.3 Increased Intracranial Pressure

After considering the effect of autoregulation mechanism failure and sympathetic nervous system dysfunction on the hemodynamic response after AVM occlusion, another factor, the influence of increased intracranial pressure(ICP) on the hemodynamic response following AVM occlusion, will also be considered. After AVM occlusion, blood from the AVM vascular bed is routed into the tissue that is unable to autoregulate effectively, resulting in hyperemia or hemorrhage, both of which have been implicated as being
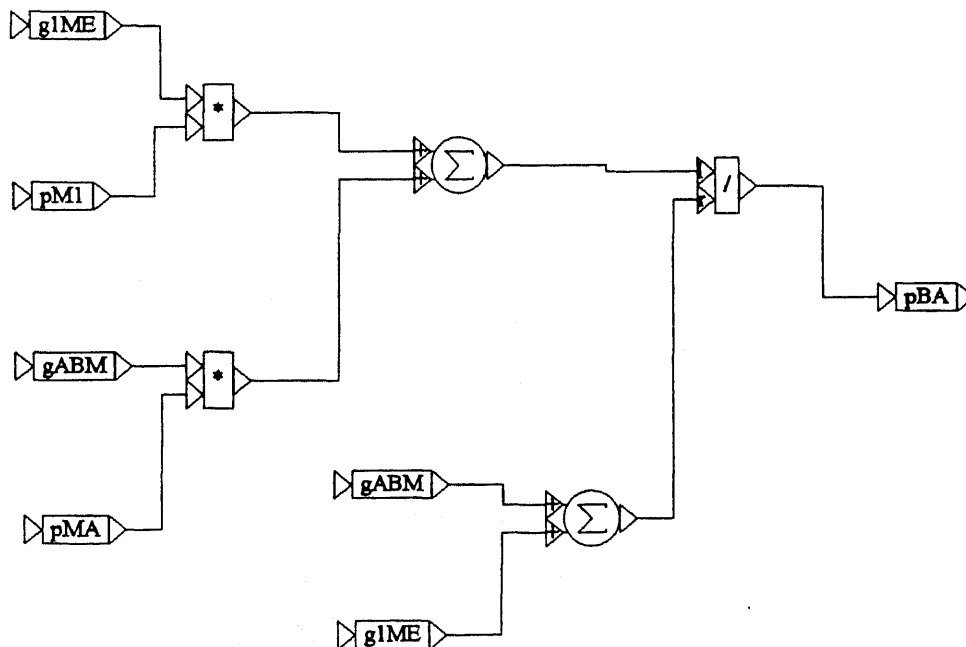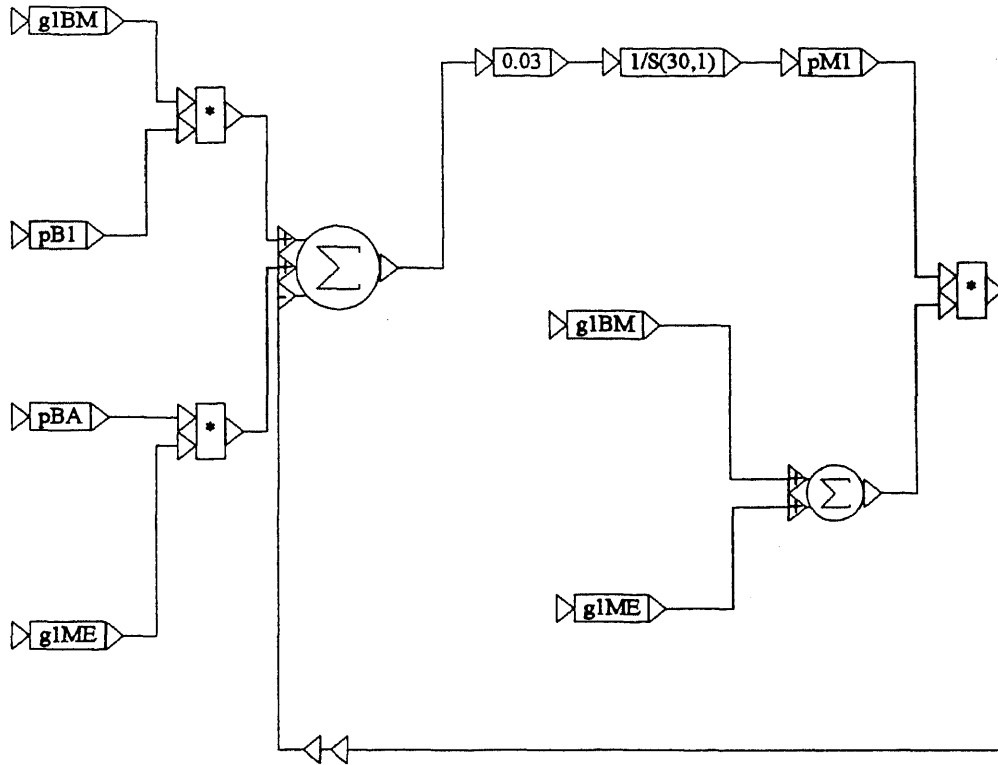
Figure 3.11 The Simulation Diagram
for the Sympathetic Branch

responsible for intracranial hypertension[15][16][17]. Now the question is whether this increased ICP will make the draining vein compress sufficiently so that the diameter of the vessel is markedly decreased, and the capillary bed further overload, resulting in more serious brain swelling or hemorrhage. To answer this question, we will simulate this phenomenon by decreasing the proximal conductance of the draining vein(Gvbm) gradually to see what will happen to the capillary pressure after AVM occlusion. We assume autoregulation in this case has a medium degree of failure. After AVM occlusion, let the proximal conductance of the drain vein Gvbm decrease gradually as shown in table 3.2. In this table, A has the biggest value of vessel conductance, and thus has the shallowest degree of vein compression, whereas E has the smallest value of vessel conductance and the deepest degree of vein compression.

The simulation was carried on the 486-PC using the same Vissim software.

Table 3.2 Different Degrees of Vein Compression

Time Interval	Gvbm
A	600
B	100
C	50
D	10
E	1

CHAPTER 4

RESULTS

With modeling and computer simulation, a set of results of hemodynamic response of cerebral circulation to AVM occlusion including different sets of influencing factors are derived.

4.1. Different Degrees of Autoregulation Failure

A set of computer simulation experiments were run and pressure tracings which represent the response to AVM occlusion with different degrees of autoregulation are shown in figure 4.1, where the Y axis represents four pressure responses(mmHg): distal feeding artery pressure(Pea), central capillary pressure(Pmc), fistula-like AVM pressure(Pmf) and the draining vein pressure(Pmv). The X axis represents time(sec). The hemodynamic response is divided into five parts: AVM unobstructed(open), AVM top(proximal) closed, AVM unobstructed again, AVM bottom(distal) closed, and AVM top & bottom closed. The model predicts that the pressure response is dependent on the site of AVM occlusion and the degree of autoregulation. Pea, Pmf, Pmc and Pmv remain almost the same with different degrees of autoregulation before AVM obstruction. After AVM proximal or distal as well as total resection,

VisSim-avm10494.vsm
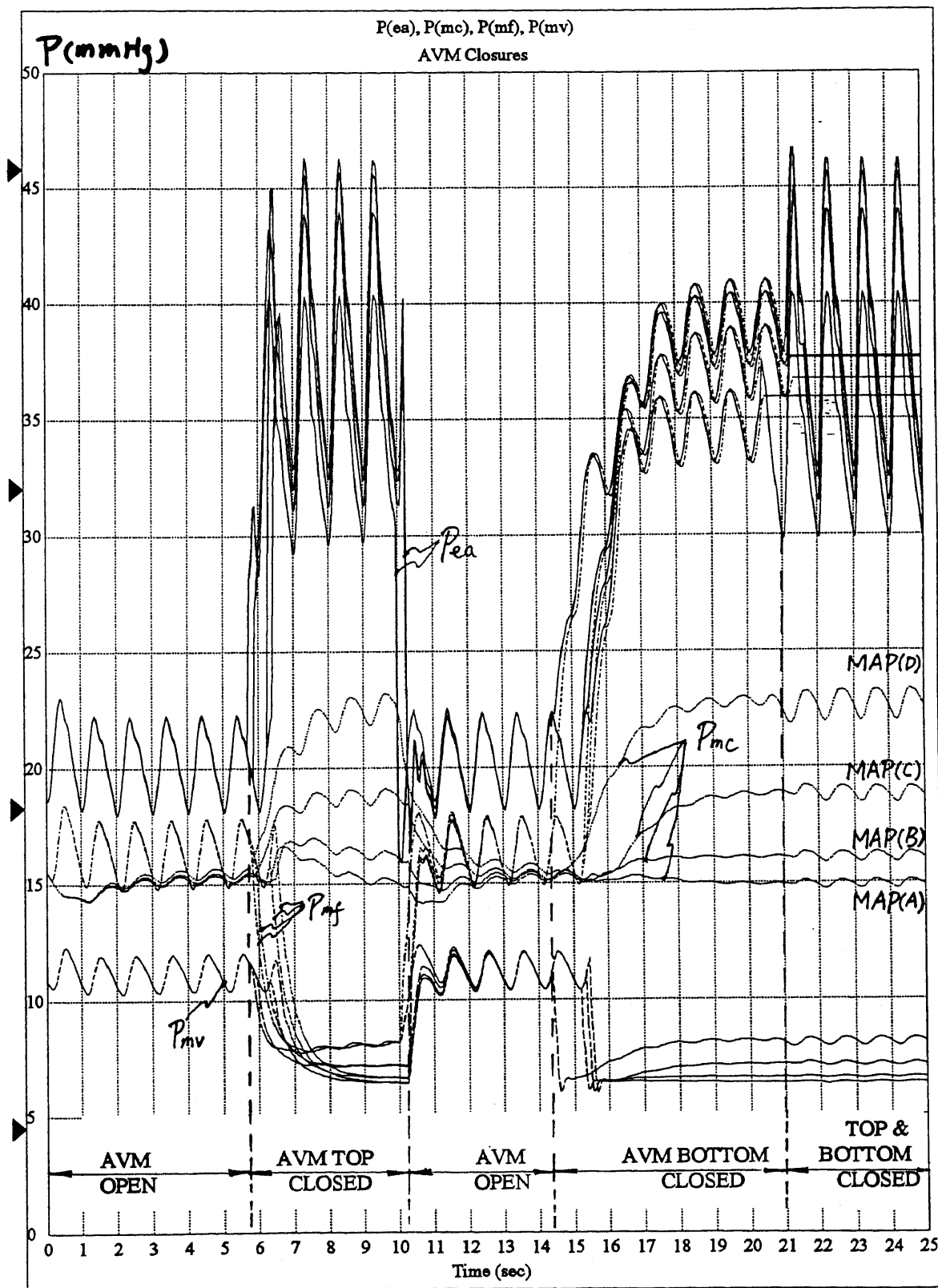
Figure 4.1 The Simulation Result of AVM System
with Different Degree of Autoregulation

capillary pressure changed significantly as shown in the Pmc curves marked with(A), (B), (C) and (D). Curves (A), (B), (C) and (D) correspond to the different degrees of autoregulation shown in figure 3.4. With normal autoregulation function (curve A), the capillary pressure remains almost constant before and after AVM proximal or distal resection. For slight autoregulation failure (curve B), capillary pressure is slightly increased. Thus the potential of capillary overload or hemorrhage is lower for either proximal and distal segment resection. For medium autoregulation failure (curve C), capillary pressure increased more, causing the probability of cerebral overload and subsequent hemorrhage to increase more. Further, the model predicts a significant increase of capillary pressure following AVM occlusion during profound autoregulation failure (curve D). The amount of capillary pressure is almost 25 mmHg, the same value as that of the system without autoregulation. This profound cerebral overload may produce severe brain swelling and subsequent hemorrhage. Fistula pressure drops rapidly after AVM proximal occlusion, whereas following AVM distal occlusion, this pressure increases to approximate arterial pressure, and may produce a chance of brain swelling and hemorrhage. Distal feeding artery pressure (Pea) also increases after AVM occlusion which has already been observed in clinics, and the draining vein pressure and pulsatality decrease at the same time.

4.2 Sympathetic Nervous System Dysfunction

An example of the simulated pressure tracings which represent the sympathetic nervous system stimulation and denervation as well as AVM occlusion is shown in figure 4.2, where four pressure tracings still represent the distal feeding artery pressure (Pea), central capillary pressure(Pmc), fistula-like AVM pressure(Pmf) and the draining vein pressure(Pmv). The result is divided into three parts. The left part represents the pressure response when the sympathetic nervous system acted normally, the middle part represents the pressure response when the sympathetic nervous system was denervated, and the right part represents the pressure response when AVM proximal resection occurs at the same time as sympathetic nervous system denervation. The results show that without considering the autoregulation mechanism, cerebrovascular pressure response is dependent on the sympathetic nervous system action. Simulated sympathetic nervous system denervation leads to an increase in distal feeding artery pressure, fistula like AVM pressure, capillary pressure and draining vein pressure with a decrease in all pressure pulsatility. The model predicts significant increase in proximal feeding artery and capillary pressure after AVM proximal occlusion with the denervation of sympathetic nerves. This increased pressure may result in hyperperfusion and subsequent hemorrhage depending on the magnitude of the pressure increase and the state of autoregulation. Fistula
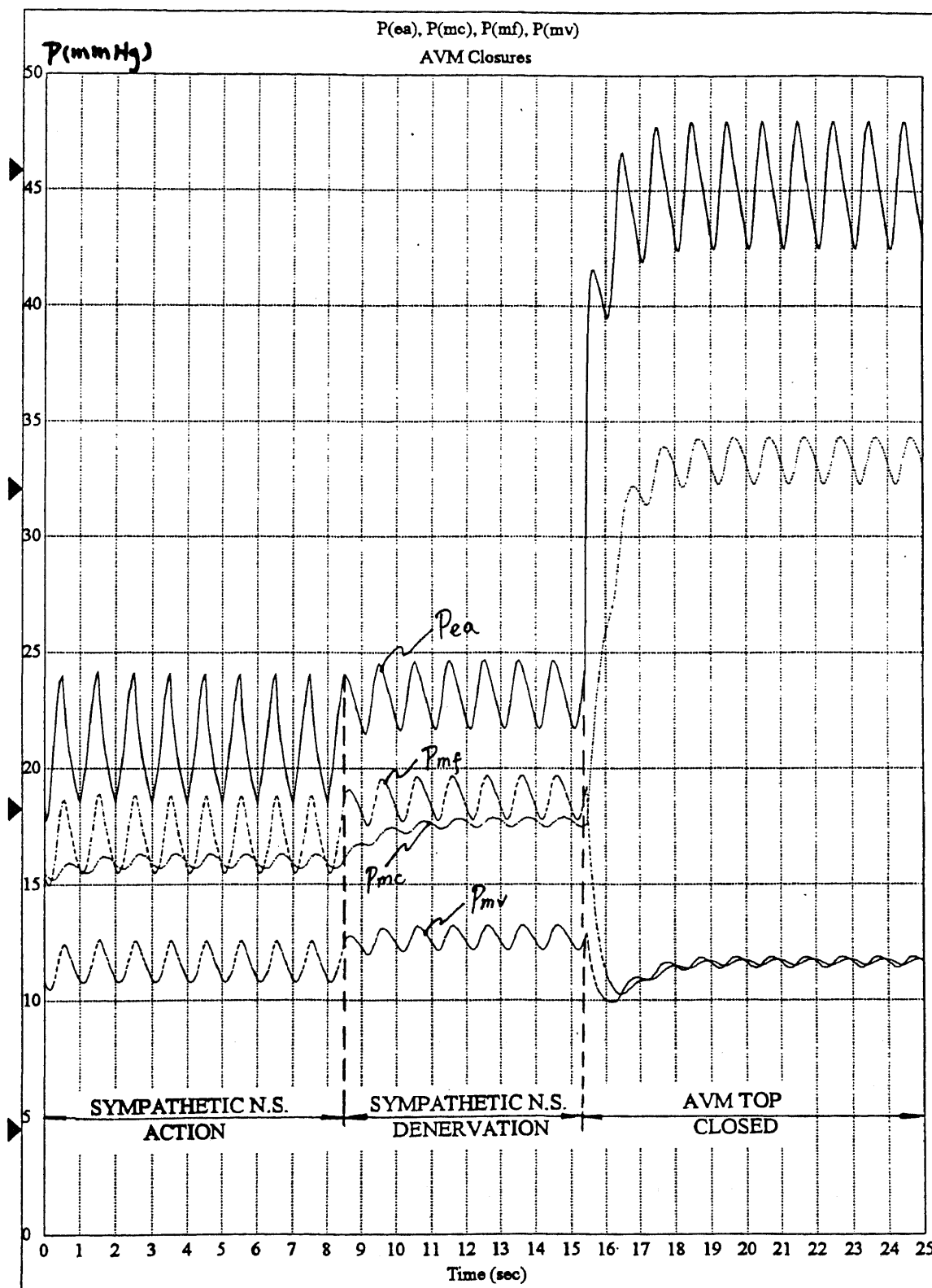
Figure 4.2 The Simulation Results of Sympathetic Nervous
System Stimulation & Denervation with AVM Occlusion

pressure rapidly falls after AVM proximal occlusion. With AVM distal occlusion, fistula pressure rises to almost the arterial pressure. This may also cause brain swelling and hemorrhage to occur. If however, the AVM patients with sympathetic nervous system dysfunction had a relatively normal autoregulation mechanism, arterial and capillary pressure will not increase as high after AVM resection, and the potential of brain swelling or hemorrhage will decrease.

4.3 Increased Intracranial Pressure (ICP)

A set of pressure tracings representing the response to different degrees of draining vein compression are shown in figure 4.3. In the figure, the four pressure tracings represent the distal feeding artery pressure(Pea), central capillary pressure(Pmc), fistula-like AVM pressure(Pmf) and draining vein pressure(Pmv). The results are divided into five time intervals marked with "A", "B", "C", "D" & "E". Each time interval is due to the compression of the vein causing a reduced conductance. The results show that the pressure response is dependent on the degrees of vein compression. The greater the compression of the draining vein, the higher the pressure response after AVM resection. During vein compression, distal feeding artery pressure(Pea) is least influenced whereas the draining vein pressure is the greatest influenced. The results also show that the average distal arterial pressure(Pea) changed a little(1.5 mmHg) when the vein conductance Gvbm decreased from 600 to

50. Capillary pressure change is greater than the change of feeding artery pressure for the same amount of Gvbm change. When Gvbm changed from 10 to 1, these two pressures increased rapidly. Further, when Gvbm equals to 1, capillary and draining vein pressure rises to almost arterial pressure, which may be the critical vessel closing point. Fistula pressure(Pmf) remains constant during the vein compression process because of the assumption that the AVM has already been closed. The ICP corresponding to the critical vessel closing pressure is about 110 mmHg[15]. This value is far beyond the actual ICP in the AVM patients[15][1][2][7]. Thus the possibility of brain swelling and hemorrhage due to the draining vein closing because of the increased ICP is very low.

Summarizing all the results, it is found that the degree of autoregulation failure is the most crucial because autoregulation occurs at the first stage regulation in the entire cerebrovascular regulation[1][2][8]. During sympathetic activation with constriction of the larger resistance vessels, the smaller resistance vessels further downstream will dilate as autoregulatory response to keep CBF constant as long as the blood pressure is within the autoregulatory range. The opposite takes place if the sympathetic tone is reduced. Only at the limits of autoregulation or at the condition of autoregulatory mechanism failure may the vasomotor function of the larger resistance vessels affect CBF because the

Figure 4.3 The Simulation Result of
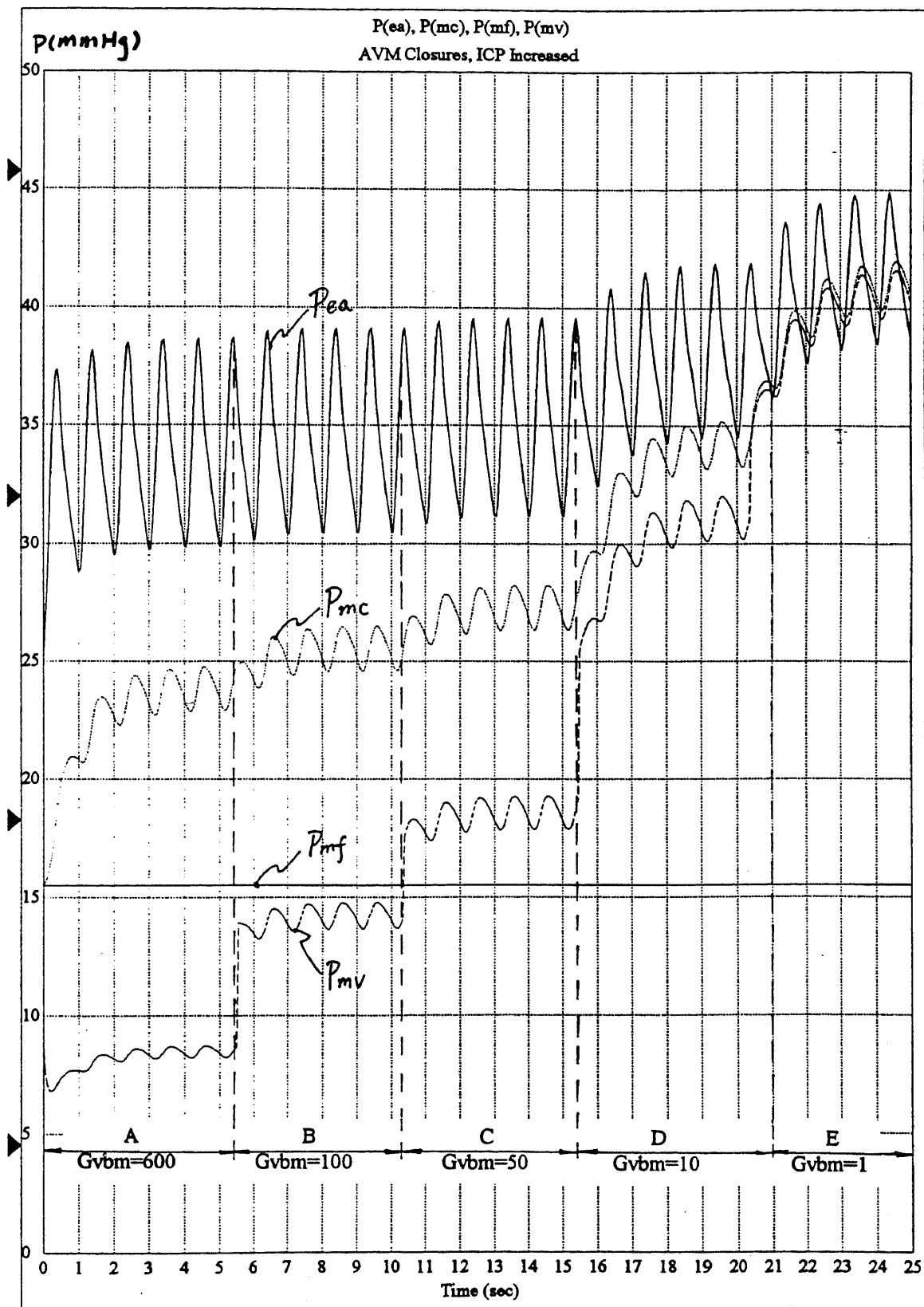Increased Intracranial Pressure

smaller resistance vessels no longer have the full autoregulatory capacity[4][8][13][14]. The factor of increased ICP is not a major problem because the ICP would have to be in the range of 110 mmHg to cause a major decrease in conductance of the draining vein and this pressure does not occur in the AVM patients which were examined for this study.

CHAPTER 5

CONCLUSION

The modeling and simulation of a cerebral arterialvenous malformation occlusion and the resulting hemodynamic response have been used to qualitatively simulate some of the observed alterations in pressure and flow resulting from AVM occlusion. The model predicts the relationship between variable degree of autoregulation and the severity of the resultant edema. The greater the failure of the autoregulation function in AVM patients, the higher the potential of hemorrhage. For patients who have normal or slight autoregulation failure, AVM proximal or distal occlusion will not result in brain swelling and hemorrhage because the capillary pressure does not change appreciably after AVM resection. Thus, acute resection of the AVM branch may not produce a problem. However for patients with profound autoregulation failure, capillary pressure will rise to almost 25 mmHg, a value existing in the system without autoregulation. This may produce high possibility of brain swelling and hemorrhage. Thus, a gradual embolization procedure for the AVM branch is suggested so that the normal capillary pressure and flow would be restored gradually. The model also showed the relationship between sympathetic nervous system dysfunction and the pressure response after AVM occlusion. The lower the sympathetic tone in AVM

57

the higher the possibility of hemorrhage. Thus, this is also a factor that should be considered in making AVM resection decisions. Increased ICP will influence the hemodynamic response following AVM occlusion depending on the magnitude of the increase. In practical situations, the ICP in AVM patients won't rise to a value that would cause the draining vein to be closed. Therefore, this factor is not significant in affecting the hemodynamic response after AVM occlusion. Mauro Ursino et al state[8][13] that the overall cerebrovascular regulation is the result of the interaction between several simpler individual subsystems mutually interdependent that superimpose their behaviors in a complex manner. For example, the sympathetic nervous system predominantly exerts its vasomotor function in the larger cerebral resistance vessels(the "inflow tract"), whereas autoregulation predominantly is a function of the smaller resistance vessels[4]. During sympathetic activation with constriction of the larger resistance vessels, the smaller resistance vessels further downstream will dilate as an autoregulatory response to keep CBF constant as long as the blood pressure is within the autoregulatory range. The opposite takes place if the sympathetic tone is reduced. Only at the limits of autoregulation may the vasomotor function of the larger resistance vessels affect CBF because the smaller resistance vessels no longer have the full autoregulatory capacity. Thus, besides investigating the effect of the individual factors, a suggestion for future

study would consider the two main factors of autoregulation failure and sympathetic dysfunction to simulate the system as the complex result of these two simultaneous mutually dependent actions. On the other hand, there are some other cerebrovascular regulatory mechanisms such as chemical mechanisms [4] [8] are also valuable to explore, which states that oxygen affects vascular smooth muscle tension and thus CVR and CBF through an indirect mechanism, mediate by the release of vasodilatory substances from tissue during hypoxia. Therefore, the other possible future study could develop some AVM models that include these other factors to investigate the relationship between the magnitude of these factors and the potential of hemorrhage.

APPENDIX

VisSim (Visual solutions Inc. Westford, MA) is a powerful computer-aided engineering(CAE) program that provides a complete visual and graphical work space for designing, simulating, and plotting models of a dynamic system. In VisSim, we build models in the form of block diagrams. Blocks and flex wires are the primary design tools. The user can wire blocks together, assign appropriate block and simulation parameters, simulate the diagram, and plot the results, all within a single interactive environment.

There are two main types of blocks in VisSim: standard blocks and compound blocks. Standard blocks include the following: (1) Annotation Blocks, (2) Arithmetic blocks, (3) Boolean Blocks, (4) Integration Blocks, (5) Nonlinear Blocks, (6) Random Generator Blocks, (7) Signal Consumer Blocks and so on. The compound blocks have the ability to encapsulate one or more blocks in a single block. With this power of VisSim, the top level blocks(compound blocks) display major component connectivity, and leave the underlying levels to describe the logic of each component. Some basic blocks also have block parameters which allow you to set simulation invariant properties of a block's function. For instance, the function of the pow block is to produce an output signal based on the value of input signal raised to the power of a specified exponent. The exponent is a parameter for the pow block. Most blocks that operate on

signals have input and output connector tabs with triangular shapes that enable the user to easily see the direction in which the signals travel. To make the simulation, flex wires are attached to blocks via their connector tabs, allowing the signals to pass from one block to the next through the flex wires. Each block can have two types of signals: input signal(Xn), which represent data entering a block, and output signals(Yn), which represent data exiting a block. VisSim has the ability to solve several types of equations, such as ordinary differential equations(ODEs). It solves the ODEs by transforming the differential equations into ones that use integration operators. Let's take an example of using VisSim software to solve a second order differential equation to show how to convert the mathematical equations into a VisSim block diagram.

Suppose a second order differential equation is expressed as:

$$A\frac{d^2y}{dt^2} + B\frac{dy}{dt} + Cy = 0$$

Because integration is inherently more numerically stable than differentiation, the next step is to express the equation in terms of integrals. By definition of the derivative:

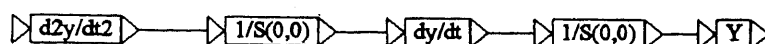$$\frac{dy}{dt} = \int_0^t \frac{d^2y}{dt^2} + \frac{dy(0)}{dt}$$

and

$$y(t) = \int_0^t \frac{dy}{dt} + y(0)$$

employing the Laplace operator 1/S as shorthand notation for integration, and making the initial conditions implicit in the 1/S operator, the following relationship results:

$$y(t) = \frac{1}{S}\frac{dy}{dt} = \frac{1}{S}[\frac{1}{S}\frac{d^2y}{dt^2}]$$

The relationship can be expressed in ViaSim block diagram form as

Here, three variable blocks hold the quantities $\frac{d^2y}{dt^2}$, $\frac{dy}{dt}$, and y at each instant of time. The variable blocks are actually extraneous, because the wires alone can carry the data forward to the next block.

Returning to the original equation, we can rewrite it as follows:

$$\frac{d^2y}{dt^2} = -\frac{1}{A}[-Cy - B\frac{dy}{dt}]$$

This is implemented in VisSim by wiring the output of the y and $\frac{dy}{dt}$ variable blocks through two gain blocks(which represent A and C) and into a summingjunction block, with inputs negated. The output of the summingjunction block is divided by A(which is represented by a constant block) to

produce $\dfrac{d^2y}{dt^2}$. Now letting B=1, C=5, and A=10, as an example,

results in the following diagram:
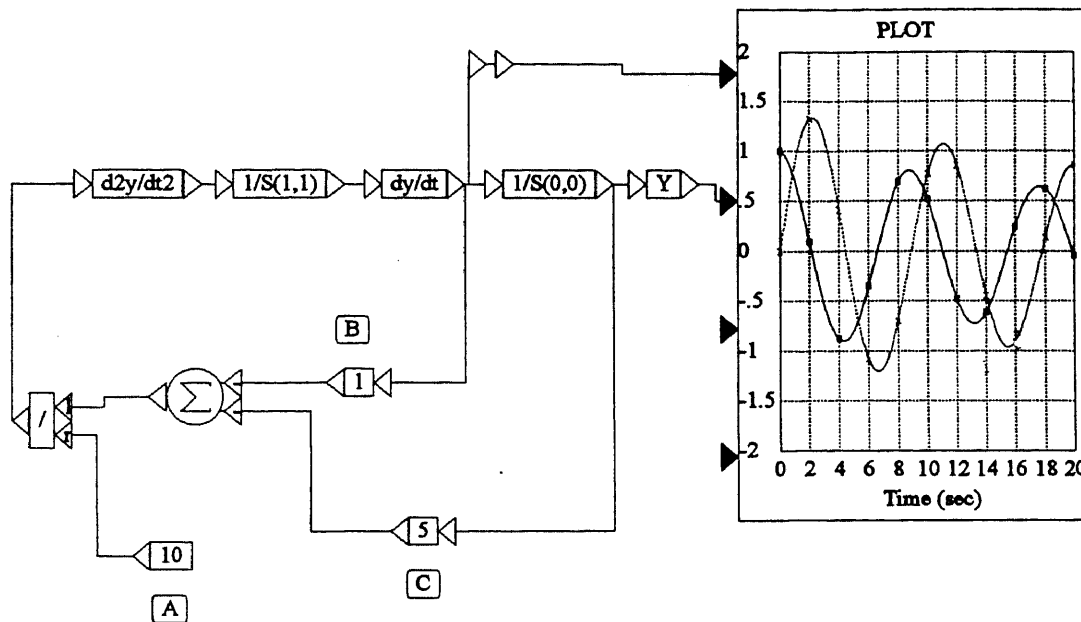
This diagram represents a closed loop system from which the

values for y(t), $\dfrac{dy}{dt}$, and $\dfrac{d^2y}{dt^2}$ can be tapped off and

displayed in a plot block, as was done here. Different

values can be entered into the appropriate blocks to

simulate any set of initial conditions or system parameters.

To build this file, the following steps can be followed:

(1). Use the File menu's New command to create a new block

diagram.

(2). Choose and insert three variable blocks to denote

$\dfrac{d^2y}{dt^2}$, $\dfrac{dy}{dt}$, and y, two gain blocks to denote B and C, a

constant block(const) to denote A, a divide(/) block,

summingjunction block, two integrator blocks and a plot
block.

(3). Establish parameter values-- such as the A, the initial
condition of 1/S, and the characteristics of the plot block.

(4). Toggle the sign on the summingjunction block's input
connector tabs to -.

(5). Wire the blocks together.

(6). Simulate the diagram.

ABBREVIATION

AVM---Arterialvenous Malformation

CVR---cerebrovascular resistance

CBF---cerebral blood flow

CPP---cerebral perfusion pressure

CVRM--the maximum value of cerebrovascular resistance for
autoregulation

CVRB--the minimum value of cerebrovascular resistance for
autoregulation

CVRD--the difference between CVRM and CVRB

NCPP--normal perfusion pressure

CL----the lowest limit of CPP for autoregulation curve

Pb1---the begining pressure of symathetic branch

Pm1---the central point pressure of symathetic branch

Pba---the begining of vessel pressure of arterial branch

Pma---the central of vessel pressure of arterial branch

Pea---the end of vessel pressure of arterial branch

Pbc---the begining of vessel pressure of capillary branch

Pmc---the central of vessel pressure of capillary branch

Pec---the end of vessel pressure of capillary branch

Pbf---the begining of vessel pressure of fistula branch

Pmf---the central of vessel pressure of fistula branch

Pef---the end of vessel pressure of fistula branch

Pbv---the begining of vessel pressure of vein branch

Pmv---the central of vessel pressure of vein branch

Pev---the end of vessel pressure of vein branch

Glbm--the proximal vessel conductance of sympathetic

branch

Glme--the distal vessel conductance of sympathetic

branch

Gabm--the proximal vessel conductance of arterial branch

Game--the distal vessel conductance of arterial branch

Gcbm--the proximal vessel conductance of capillary branch

Gcme--the distal vessel conductance of capillary branch

Gfbm--the proximal vessel conductance of fistula branch

Gfme--the distal vessel conductance of fistula branch

Gvbm--the proximal vessel conductance of vein branch

Gvme--the distal vessel conductance of vein branch

REFERENCES

1. Ornstein E. Blesser W.B. Young W.L. Fleischer L.H. Spellman J.P.: "Hemodynamic Effects of Intracranial Arteriovenous Malformation Occlusion: A Computer Simulation." Proceedings of the 14th Conference, IEEE Engineering in Medicine and Biology Society, 1993, pgs. 548-549.

2. Young W.L. Solomon R.A., Prohovnik I., Ornstein E., Weinstein J., Stein B.M.: "133Xe Bood Flow Monitoring dring Ateriovenous Maformation Rsection: A Case of Intraoperative Hyperfusion with Subsequent Brain Swelling." Neurosurgery, vol. 22 1988, pp.765-769.

3. Young W.L., Prohovnik I., Ornstein E., Sisti M.B., Solomon R.A., Stein B.M. Ostapkovich N.: " Monitoring of Intraoperative Cerebral Hemodynamics before and after Arteriovenous Malformation Resection." Anesth Analg 1988, vol.67 pp.1011-14.

4. Paulson O.B., Strandgaard S., Edvinsson L.: "Cerebral Autoregulation." Cerebrovascular and brain metabolism, Rev. vol.2, no.2, 1990.

5. Hoffmann O.: "Biomathematics of Intracranial CSF and Hemodynamics. Simulation and Analysis with the Aid of a Mathematical Model." Acta Neurochirurgica. Suppl. 40, 1987 pp.117-130.

6. Nornes H. , Grip A. , Wikeby P.: "Intraoperative evaluation of Cerebral Hemodynamics using Directional Doppler Technique.Part 1. Arteriovenous Malformations." J Neurosurg, vol.50, 1979, pp.145-51.

7. Ornstein E., Blesser W.B.: "Evolution of AVM Model." Private Communication.

8. Ursino M. : "A Mathematical Model of Overall Cerebral Blood Flow Regulation in the Rat." IEEE Transactions on biomedical Engineering, vol.38. no.8, Aug. 1991, pp.795-807.

9. Nornes H., Grip A.: "Hemodynamic Aspects of Cerebral Arteriovenous Malformations." J Neurosurg. vol.53, 1980, pp.456-464.

10. Lo E.H., Fabrikant J.I., Levy R.P., Phillips P.H., Frankel K.A., Alpen E.L.: "An Experimental Compartmental Flow Model for Assessing the Hemodymanic Response of Intracranial Arteriocenous Malformations to Stereotactic Radiosurgery." Neurosurgery, vol.28, no.2, 1991. pp.251-259.

11. Pucher R.K., Auer L.M. : "Effect of Vasospasm in the Middle Cerebral Artery Territory on Flow Velocity and Volume Flow.A Computersimulation." Acta Neurochir, vol.93, 1988, pp.123-128.

12. Edvinsson L., Owman C., Siesjo B.: "Physiological Role of Cerebrovascular Sympathetic Nerves in the Autoregulation of Cerebral Flow." Brain Research, vol.117, 1976, pp.519-532.

13. Baumbach G.L., Heistad D.D.: "Effects of Sympathetic Stimulation and Changes in Arterial Pressure on Segmental Resistance of Cerebral Vessels in Rabbits and Cats." Circulation Research, vol.52, no.5, 1983, pp.527-533.

14. Harper A.M., Deshmukh V.D., Rowan J.O., Jennett W.B.: "The Influence of Sympathetic Nervous Activity on Cerebral Blood Flow." Arch Neurol, vol.27, 1972, pp.1-5.

15. Lowell H.M., Bloor B.M.: "The Effect of Increased Intracranial Pressure on Cerebrovascular Hemodynamics." J. Neurosurg., vol.34, 1971, pp.760-769.

16. Johnston H., Rowan J.O.: "Raised intracranial Pressure and Cerebral Blood Flow." J. of Neurology, Nerusurgery, and Psuchiatry, vol.37, 1974, pp.392-402.

17. Langfitt T.W., Weinstein J.D., Kassell N.F., Gagliatdi L.J., Shapiro H.M.: "Compression of Cerebral Vessels by Intravranial Hypertension.I. Dural Sinus Pressure." Acta Neurochirurgica, vol.xv, Fasc.3-4, pp.213-222.

18. Shapiro H.M., Langfitt T.W., Weinstein J.D.: "Compression of Cerebral Vessels by Intravranial Hypertension.II. Morphological Evidence for Collapse of Vessels." Acta Neurochirurgica, vol.xv, Fasc.3-4, pp.223-233.

19. Heistad D.D., Marcus M.L.: "Evidence that Neural Mechanisms do not have Important Effects on Cerebral Blood Flow." Circ.Res., vol.42, 1978, pp.295-320.